TAMPEREEN TEKNILLINEN YLIOPISTO
TAMPERE UNIVERSITY OF TECHNOLOGY

OLLI-PEKKA KARJALAINEN

CAPACITIVE MEASUREMENT FOR ROBOT Z-AXIS POSITION

Master of Science thesis

Examiners: Professor Risto Ritala
and Professor Jose Martinez Lastra
Examiner and topic approved by the
Faculty Council of the Faculty of
Engineering Sciences
on 7th December 2016

ABSTRACT

OLLI-PEKKA KARJALAINEN: Capacitive measurement for robot z-axis position
Tampere University of Technology
Master of Science Thesis, 52 pages, 1 Appendix pages
April 2017
Master's Degree Programme in Automation Technology
Major: Factory Automation and Industrial Informatics
Examiners: Professor Risto Ritala and Professor Jose Martinez Lastra

Keywords: capacitive, measurement, force, robotics, tactile sensing

This Master of Science thesis presents mechanical, electrical, measurement and software design and implementation for robot end effector with capacitive tactile force sensor. This end effector is designed to measure both touch and force in z-axis direction and then used in automated testing of smart devices.

Various mechanical and electrical designs can be used in the design of a tactile force sensor. The chosen design is always application driven. Selection of measurement technology and decisions made during the design are dependent on the use case and the demands of the application. Different technologies are introduced and one of them is chosen. The selection is justified on the base of preferred attributes.

The designed tactile sensor, with changeable spring steel flexure sheets, is a proof of concept that force sensing can be made affordable and capacitive technology can be used in it. The sensor with 0.1 mm thick spring steel flexure pair is capable to measure forces from 0 g to 70 g with resolution of 2.36g, precision of 1 g, hysteresis of 0.5% and linearity error of ± 1%. In touch sensing of the surface in the direction of z-axis, the sensor performs reliably under 3 milliseconds.

In force sensing, the previously used methods have always leaned towards commercial solutions which are often expensive and the new design offers an alternative option for this. Also, implementing of any commercial force sensor to a robot tool needs always mechanical, electrical and software work. With this new design, the flexure mechanics and sensor is already implemented in the tool.

The previous method for sensing touch with the surface based on postprocessing of collected data. And by this old method, the touch event information did not perform in real time. With the new design, results closer to this demand were achieved.

TIIVISTELMÄ

OLLI-PEKKA KARJALAINEN: Kapasitiivinen mittaus robotin z-suuntaiseen positioon
Tampereen teknillinen yliopisto
Diplomityö, 52 sivua, 1 liitesivua
Huhtikuu 2017
Automaatiotekniikan diplomi-insinöörin tutkinto-ohjelma
Pääaine: Factory Automation and Industrial Informatics
Tarkastajat: Professori Risto Ritala ja Professori Jose Martinez Lastra

Avainsanat: kapasitiivinen, voimamittaus, kosketusmittaus, robotti,

Tämän diplomityön aiheena on kapasitiivinen mittaus robotin z-akselin suuntaiseen positioon. Työssä käydään läpi mekaaninen, sähköinen, mittaustekninen ja ohjelmallinen suunnittelu sekä toteutus. Suunnittelun ja toteutuksen tavoite oli tuottaa kohtuuhintainen, kapasitanssiin perustuva voima-anturi ja tutkia sen ominaisuuksia sekä käyttökelpoisuutta kosketusnäyttöjen ja älylaitteiden testauksessa.

Kosketukseen perustuva voimamittaus on mahdollista toteuttaa useilla eri tavoilla, niin mekaanisesti kuin sähköisestikin. Valittu suunnittelupolku on kuitenkin aina käyttökohteesta ja sen asettamista vaatimuksista riippuvainen. Useita eri teknologioita on mahdollista implementoida ja tässä työssä on käyty läpi niistä yleisimmät sekä valittu perustellusti yksi.

Suunnittelun tuloksena syntynyt sensori ja sen mekaniikka koostuvat kapasitiivisesta parista ja vaihdettavasta jousiteräslevyistä. Kokoonpano 0.1 mm vahvuisilla jousiteräslevyillä on kykenevä mittaamaan voimia väliltä 0-70 g, resoluutiolla 2.36 g, toistotarkkuudella 1 g, hystereesillä 0.5% ja lineaarisella virheellä 1%. Pinnantunnistuksessa puolestaan kyseinen kokoonpano suoriutuu luotettavasti alle 3 millisekunnissa.

Aikaisemmin käytetyt metodit ja suunnitelmat voimamittauksissa ovat nojanneet kaupallisiin voimasensoreihin. Ne ovat usein kalliita ja tämä tutkimus tarjoaakin vaihtoehdon kaupalliselle sensorille. Aikaisemmat metodit kosketuspinnan tunnistukseen perustuivat kerätyn datan jälkikäsittelyyn eikä siten toimineet reaaliajassa. Uudella kokoonpanolla päästään jo hieman lähemmäksi tätä vaatimusta.

PREFACE

This Master of Science thesis is made to Optofidelity. It is based on the idea originally presented by Tommi Björk, to whom I owe special thanks for mentoring and organizing the possibility for this thesis work.

Design, implementation and measuring of the capacitive tactile force sensor was extremely educational and provided valuable information. Writing of thesis was not always so straightforward, sometimes I spent weeks without progress while being busy with full time work or moving to another apartment. Then there were times when I could progress many pages a day.

I want to thank Dr. Janne Honkakorpi for guiding me through the tricky situations with Beckhoff hardware configuration and Teemu Pöyhönen for providing support with measurements. I also want to thank Professor Risto Ritala for examining this thesis.

The greatest thanks belong to my wife Minna, you have been there for me through my long road of studies and given me support in every step. I promise, this will be the end of it, at least until I find something else.

Finally, I want to thank my parents for encouraging and supporting in my studies. There were times when those food baskets meant the world to me.

Tampere, 18.4.2017

Olli-Pekka Karjalainen

CONTENTS

APPENDIX A: Illustration of designed tool

LIST OF FIGURES

LIST OF SYMBOLS AND ABBREVIATIONS

A	Surface area
ADC	Analog to Digital Converter
BJT	Bipolar Junction Transistor
C	Capacitance in Farads
CCD	Charge-coupled device
CMOS	Complementary metal–oxide–semiconductor
DUT	Device Under Test
D	Outer diameter
d	Inner diameter
EMI	Electromagnetic Interference
ε	Calculated dielectric constant
εr	Relative permittivity of material
ε0	Relative permittivity of vacuum
FBG	Fiber Bragg Grating
FSR	Force Sensing Resistor
GMA	Geometric Moving Average
I2C	Serial computer bus
IC	Integrated circuit
MEMS	Microelectromechanical systems
PLC	Programmable Logic Controller
PCB	Printed Circuit Board
PLA	Polylactic acid
R	Radius
RMS	Root Mean Square

1. INTRODUCTION

Tactile sensing covers all methods in which a sensor comes into physical contact with the sensed object. For this reason, tactile force sensing is also called sensing by contact. With tactile sensing, variables such as position, pressure, temperature and shape can be measured. Tactile sensing has a short range, and measurement data needs to be analyzed and processed to extract the useful information. However, short-range sensor data obtained by touch is reliable information and ideal for locating obstacles, measuring force, or detecting a touch on the surface of a screen.

Selecting the right method of transduction for tactile sensing application can be difficult. Large variety of technologies can be applied, and each technology comes as a number of devices from different vendors. These technologies need to be narrowed down by comparing them with respect to a common ground and the intended application. Resistive, capacitive, inductive, piezoelectric, magnetic, optoelectrical and ultrasonic technologies are the options for tactile sensing. These technologies are first reviewed and their advantages and disadvantages are listed. Preferred attributes for a force sensor is low price, high sensitivity, small size, simple to use, and robustness. Based on the technology analysis, a tactile force sensor for touch screen testing tool is developed in this thesis.

The thesis has been divided into Chapters as follows. Chapter 2 provides the necessary background for the technologies in tactile force sensing. Chapter 3 categorizes and evaluates the introduced technologies and provides the ground for the chosen technology. Chapter 4 introduces the mechanical design of the sensor developed, and presents the first measurements. Chapter 5 presents the electrical design and the frequency response of the sensor. Chapter 6 introduces the measurement system hardware and the software developed. Chapter 7 evaluates the sensor based on the measurements and theory from the previous chapters. Finally, Chapter 8 summarizes the research.

This research was made for Optofidelity. It is a technology company located in Tampere and founded in 2005. Optofidelity designs and delivers demanding and customized test and measurement systems for smart devices. Robotic test solutions range from plug-and-play instruments to fully customized, complex test systems through the product life cycle from R&D to production and refurbishing.

2. TACTILE FORCE SENSING TECHNOLOGIES

This Chapter gives an overview, with examples and operating principles, on tactile force sensing. First the technologies are introduced and mechanisms of transduction are explained. The technologies are evaluated for suitability in a robot's force-sensing tool. The technology review in this Chapter is based on reference [1], unless otherwise stated.

2.1 Whiskers or antenna

Whisker sensors are simple and they can provide information about close proximity of objects. Whiskers are more commonly used in mobile robotics and in research of a rodent-like robotics. As they provide information only about a single contact point, their information bandwidth is low, and makes them unsuitable for fast manipulation tasks.

Whiskers can provide information if contact occurs or not and if so, the contact location [2]. A simple whisker sensor can be made from a piano wire passing through a metal tube. Other end of the whisker would be insulated and electrical circuit is completed when the whisker touches an object. Location of the object can be calculated from the contact information combined with known coordinates in robot space. An example of a limit switch with a whisker end effector is illustrated in Figure 1.

Figure 1. *Honeywell limit switch with a spring wire [3]*

2.2 Mechanical displacement sensor

These sensors are based on mechanical displacement caused by the applied force. A simple example is a sensor consisting of a spring-loaded displacement pin, which activates micro switches as force is applied. The force required to operate micro switches is determined by the mechanical characteristics and external constraints of the assembly.

Mechanical displacement sensor does not define nor limit the technology behind the sensor. It can be viewed as a category where it expresses a way to implement sensor mechanics. Mechanical displacement sensor is discussed here because sensor assembly designed and implemented in this thesis can be categorized as one. Illustration of this design is given in Figure 2.

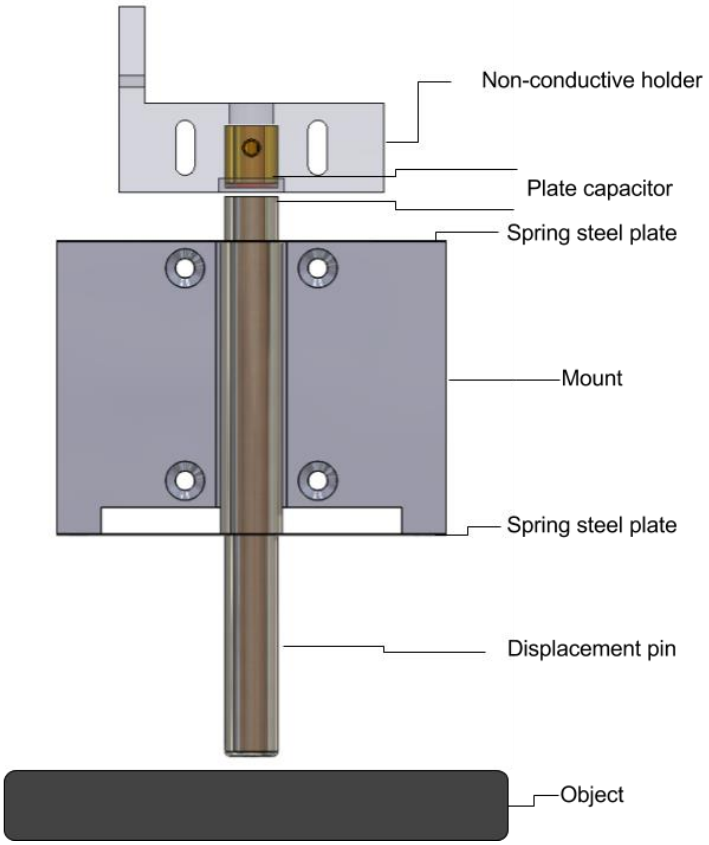

Figure 2. *Mechanical displacement sensor mechanics*

2.3 Force-sensitive Resistor

A force-sensitive resistor (FSR) is a sensor where the resistance changes as a function of applied pressure. FSR sensors typically involve two conductive sheets, which are separated by air or insulating material. There is a voltage over the sheets and when pressure is applied, the second sheet becomes in contact with the first sheet, and the sheets serve as a slide of a potentiometer. These sensors are sensitive and inexpensive but their power consumption may become an issue. Figure 3 shows a flexible force-sensitive resistor made by Uneo [4].

Although FSR can detect weight, it is not a good choice for measuring how much weight is applied. In this sense, more appropriate name would be a pressure-sensitive sensor, since the output is directly proportional to the area of the surface where force is applied. It should be noted that sensors genuinely based on resistance are much harder to find than their counterparts which use piezoresistive technology.

Figure 3. *Uneo force sensing resistor (piezoresistive) [4]*

2.4 Strain gauges

Strain gauges can be used to measure how much material shrinks or stretches in response to an applied force, torque, or stress. They are commercially widely used. Strain gauges can be either resistive or semi-conductive, which are both described below.

2.4.1 Metal strain gauge

Common metal strain gauge is made from a conductive foil pattern, which is covered with flexible insulation material. Strain gauge is attached to an object with a carefully chosen adhesive and while the object becomes under stress the foil is deformed causing its electrical resistance to change. The change of resistance is usually measured by a Wheatstone bridge circuit. The resistance change is related to the strain by the device-specific quantity known as the gauge factor (GF):

$$GF = \frac{\Delta R/R}{\varepsilon} \quad (1)$$

Here ΔR is the change in the strain gauge resistance, R is the unstrained resistance of the strain gauge, $\varepsilon = \frac{\Delta L}{L}$ is strain where ΔL is absolute the change in length, L is the original length, v is Poisson's ratio and ρ is resistivity. Gauge factor for metallic strain gauges can be typically between 2 to 5 [1][5][6]. Figure 4 illustrates a strain gauge with s-beam mechanics.

Figure 4. *Futek LSB200 resistive strain gauge [7]*

2.4.2 Piezoresistive Strain Gauge

Piezoresistive strain gauges and metal strain gauges are much alike, but made of semi-conducting material, such as silicon or germanium. Their working principle is the same as that of resistive strain gauges. However, due to use of semi-conductive materials, they can achieve much higher gauge factors. This results in a higher sensitivity to deformation and less noisy output signal. The gauge factor is a combination of a geometric part and a material-specific part:

$$GF = \frac{\Delta\rho/\rho}{\varepsilon} + 1 + 2v \quad (2)$$

Here ε is strain, $\Delta\rho$ is change in resistivity, ρ is resistivity in rest and v is Poisson's ratio, which is the relative change in lateral relations of an object. The total change in resistance of a piezoresistive strain gauge can be two orders of magnitude higher than that of a metallic strain gauge, i.e. as high as 200. However, they are not as robust as their metal counterparts [1][5].

2.5 Piezoresistive tactile sensors

Piezoresistive sensors are also available in many other forms, such as microelectromechanical (MEMS) accelometers and force sensors. These sensors are based on piezoresistivity of the material, and their working principle is much like that of a piezoresistive strain gauge. Piezoresistive effect is present in materials such as silicon carbide, single crystal silicon and germanium. Although piezoresistive sensors are more sensitive, they can be more difficult to handle in precision measurements than their metal counterparts because semiconductors are more sensitive to environmental changes; temperature and mechanical wear [1][8][10]. Figure 5 shows a FlexiForce A101 piezoresistive force sensor made by Tekscan.

Figure 5. *FlexiForce A101 Sensor [8]*

2.6 Piezoelectric tactile sensors

Piezoelectric sensors are based on piezoelectricity of materials. In contrast to the piezoresistive effect, the piezoelectrical effect causes a change in electrical potential, not electrical resistance. Piezoelectric material is a class of dielectric materials that can be polarized by applying either an electric field or mechanical stress. This unusual property is more commonly called pressure electricity. Piezoelectric materials can be divided into polar and non-polar piezoelectric materials.

A force can be applied to a load sensor as shear, transversal and longitudinal load, and the generated voltage is directly related to applied force. Sensors made with this technology are so sensitive that they can be used in microphones, in which acoustic pressure variations are transferred into voltage. Piezoelectric sensors can be also used in vibration, shock and surface level measurements. Piezoelectric effect works also the other way around: when an electrical charge is applied to the polarized crystal, it causes a mechanical deformation which in turn can be used as micro actuator or a piezoelectric speaker [1][10].

Figure 6. *Piezoelectric accelometer from Noliac [9]*

For example, a piezoelectric force sensor can be made from a polarized crystal of quartz which is placed between two metal plates forming a capacitor. An external force causes the crystal to deform, which results in an electrical charge. This electrical charge is a function of the applied force. Within the operation limits, a greater force means greater surface charge. Piezoelectric sensors can achieve very high dynamic ranges, up to 4000:1, while applying a load of 0.01-40N. The downside of the piezoelectric effect is that constant pressure cannot be measured as the sensor output decays to zero. Therefore, these sensors are best used in dynamic force measurement applications.

Materials in piezoelectric sensors are usually highly pyroelectric, see the next subsection. Problem with materials which are both pyroelectric and piezoelectric is that distinguishing the consequences of the two effects from one another can be difficult. This means that the piezoelectric sensors are highly sensitive to temperature, and thus must be protected from thermal variations.

2.7 Pyroelectric tactile sensors

Heating or cooling pyroelectric sensors generates temporarily voltages. However, when the temperature stabilizes to a new value, the pyroelectric voltage disappears due to limits of electronics. In force sensors, this effect is utilized as the sensor touches an object surface, heat is transferred from the sensor into the object or vice versa and this temperature change can be detected as a transient voltage. Pyroelectric sensors are not very good at measuring forces, but pyroelectricity must be taken into account, when designing an assembly with piezoelectric sensors.

2.8 Optical tactile force sensors

Sensors that operate by optical transduction methods employ a light source, a transduction medium and a photodetector. The operating principles of optical-based sensors can be divided into two categories:

1. Intrinsic, on which the light phase, intensity or polarization of transmitted light is modulated without deflecting the optical path.
2. Extrinsic, on which the applied force or pressure deflects the path.

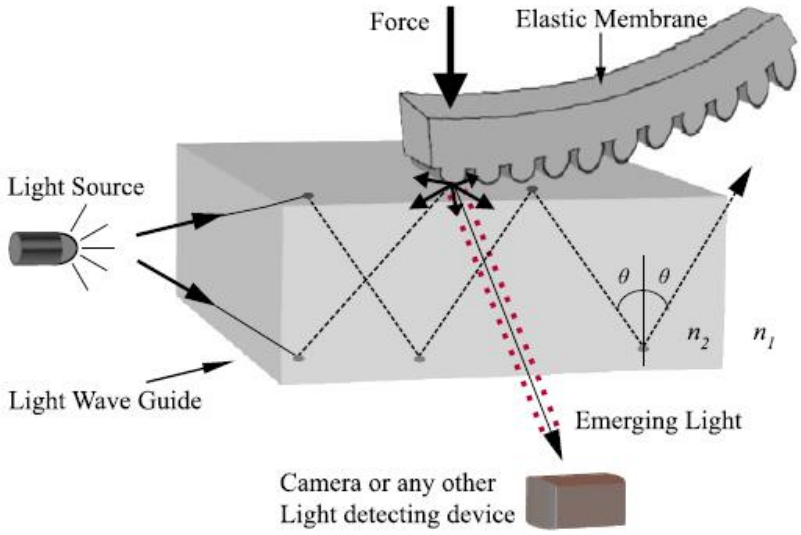

Figure 7. *Micro bending of intrinsic optical sensor [1]*

Both methods are suitable for measuring touch, torque and force but require different amount of optical and/or signal processing, depending on the technique.Intrinsic method can be described with a light source, which is projected between a clear plate and a membrane. Light is projected along the plate and total internal reflection occurs when no force is applied. However, when force is applied, the reflection is diffused. Complementary metal–oxide–semiconductor (CMOS) camera captures the diffusion and records the reflection in the imaging area. Figure 7 illustrates the intrinsic method. The intensity of the light (bright or dark areas in the image) is proportional to the magnitude of the pressure between the object and the plate. A weakness of these tactile sensors is the large consumption of current by various components.

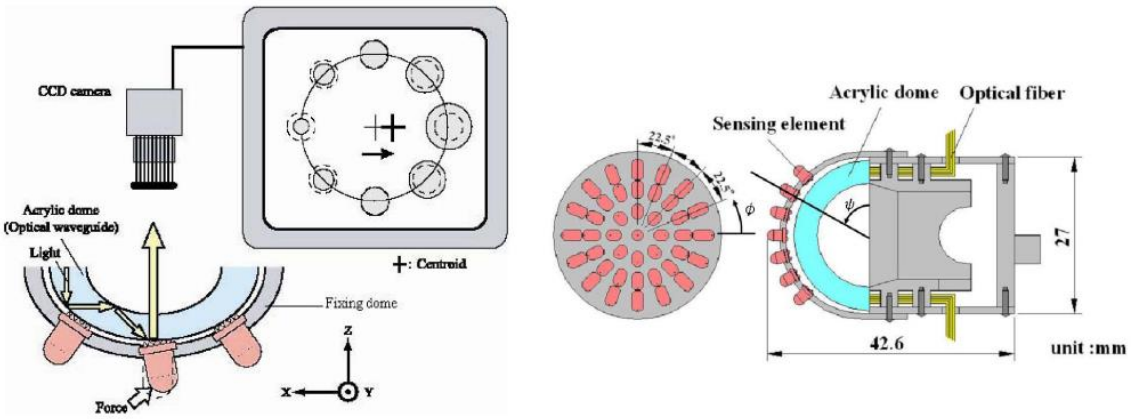

Figure 8. *Illustration of three axes intrinsic tactile sensor system [11]*

Intrinsic sensors can also be made sensitive to shear forces by appropriate design. E.g. M. Ohka, H. Kobayashi, J. Takata and Y. Mitsuya developed a three-axial tactile sensor based on an optical waveguide [11]. The sensing arrangement is dome-shaped, resembling the structure of a human fingertip, see Figure 8. Sensor consists of an array of 41 sensing elements made from silicon rubber, a light source, an optical fiber-scope and a charge-coupled device (CCD) camera. The silicone rubber element contains one barrel-shaped finger, the other end of which has eight cone shaped elements. When the sensor meets an object, the finger deforms. At the locations where the cone-shaped elements deformed, light is diffusely reflected out of the reverse surface of the waveguide. The deformed fingers are observed as bright spots in the image data. The normal force values are calculated based on integrated gray-scale value, while shearing force is calculated based on horizontal center point displacement. The sensor can measure normal and shear forces in the range 0–2 N, with a resolution of 0.001 N [1][11].

Extrinsic method has a light source, an optical shutter and a light detector. The head of the elastic membrane concentrates the force and the bar acts as the optical shutter which limits light transmission between emitter and detector. The pattern of light changes depending on the amount of force applied and thus the applied force can be calculated. Optical tactile sensors are immune to electromagnetic interference, they have high spatial resolution, and are flexible, sensitive and fast. Major disadvantages are lack of robustness, amount of image processing, and the implementation can be costly. Figure 9 illustrates an extrinsic method.

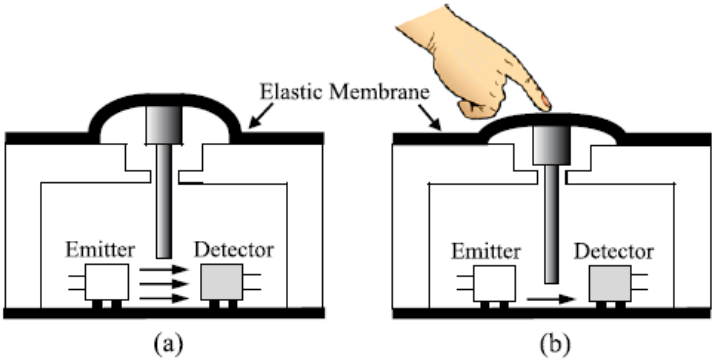

Figure 9. *Extrinsic method with emitter and detector [1]*

The sensors based on fiber Bragg grating (FBG) are extrinsic optical sensors. The FBG based sensor system monitors the wavelength shift of the returned Bragg-signal. The wavelength shift is a function of the parameter to be measured, such as strain in a strain gauge or force of capacitive load cell. E.g. The 3 × 3 tactile sensor researched by J. Heo, J. Chung and J. Lee studied a 3 × 3 tactile sensor based on FBG [12]. This sensor measures normal forces as little as 0.001 N with the spatial resolution of 5 mm.

These examples of sensors, both intrinsic and extrinsic ones, have been designed for human skin-like tactile sensing. Sensitivity and resolution in these examples are high, but the dynamic range is rather limited. As these sensors are designed for other purposes of tactile sensing, although very accurate they do not fit into the needs of repeated, robust, inexpensive touch screen testing, the objective of this thesis.

2.9 Ultrasonic tactile sensors

Ultrasonic tactile sensors are acoustic sensors, which are good in detecting small movements during contact, such as slipping of a gripped object. Ultrasound has more commonly been used in measuring the thickness of an object. However, in tactile sensing, ultrasonic sensors are used similarly: the time it takes an ultrasonic pulse to travel through material and return after reflection is measured. When the propagation speed of ultrasonic wave in the material is known, the material thickness can be calculated. By applying this principle, the thickness of a flexible elastomer layer can be measured at many closely spaced points and the pressure applied on the surface can be calculated. Illustration of the method is in Figure 10.

The ultrasound is generated with a piezoelectric speaker which transmits a pulse of few megahertz into a rubber pad. The reflected echo is received usually by the generating element. Unfortunately, ultrasonic sensors cannot measure force if the target material has same acoustic properties as the sensor skin material. Ultrasonic sensors are not commonly used in force sensing, partially due to the simpler technologies discussed in this Chapter. Difficulties with ultrasonic sensors in miniaturized circuits are also reported [1][10].

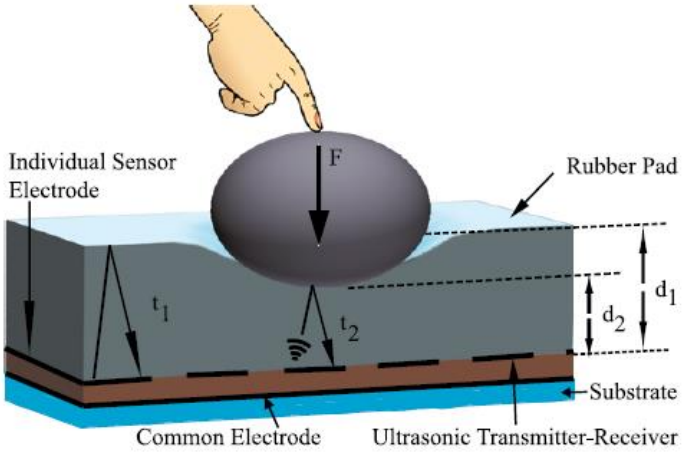

Figure 10. *Ultrasonic method illustration [1]*

2.10 Magnetic tactile sensors

Magnetic tactile sensor applies two approaches. The first approach is to measure changes in the magnetic flux either by Hall effect, illustrated in Figure 11, or by magnetoresistance. The second approach is to measure the change in the magnetic coupling or change in the inductance of a coil. In Hall effect, the charge carriers flowing through a conductive material, in presence of a magnetic field, experience a force orthogonal to both their flow direction and the magnetic field direction. Thus, the charge carriers are deflected, leading to the appearance of Hall potential in the direction of the deflection.

Hall effect based tactile sensors have high sensitivity, low hysteresis, linear response, wide dynamic range, and are robust. However, they are very sensitive to magnetic interference and noise. This means that they cannot be used in magnetic environments [1][10].

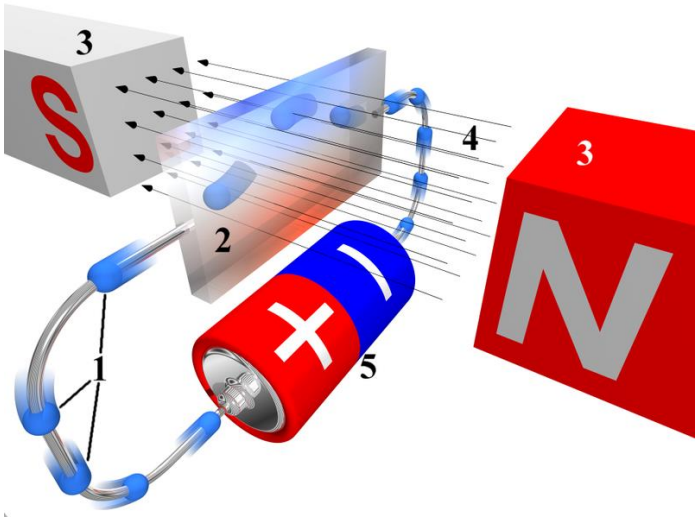

Figure 11. *Illustration of Hall effect [13]*

2.11 Capacitive sensors

Physical quantities, such as distance, pressure, acceleration, humidity, liquid level and material composition have been measured for a long time by capacitive sensors. More recent applications of capacitive touch technology are displays of computers, mobile phones and other smart devices. Capacitive technology is also widely used in MEMS based touch sensing arrays such as high resolution tactile imaging of fingerprints in smart devices. These techniques have also been employed in robotics to detect contacts over large areas of a robot's body.

Capacitance is the ability of a system to store electrical charge. Any capacitive sensing system consists of a set of conductors that interact with electric field. Typically, the capacitive sensors are the plate capacitors, see Figure 12, which have two identical and parallel metal plates as electrodes. These metal plates have an area A and are separated by a distance d by a flexible spacer. This spacer is usually silicone or air and have some relative dielectric constant εr. The capacitive sensor detects the change in capacitance when the sensor is approached or touched. The capacitance of a parallel-plate type capacitor is

$$C = \varepsilon_r \varepsilon_0 \frac{A}{d} + C_f \tag{3}$$

Here C is the capacitance, ε_r is the relative permittivity and represents the ability of a material to store electrical energy in the presence of an electric field, ε_0 is the electric permittivity of vacuum and C_f is the contribution from edges of the electrode which tend to store more charge than rest of the electrode. Typically, $A \gg d^2$ so C_f term is trivial. From previous equation, a simplified formula for parallel plate capacitor can be formed: $C = \varepsilon A/d$, where $\varepsilon = \varepsilon_r \varepsilon_0$.

Figure 12. *Basic principle of capacitance and iLoad mini load cell [14]*

The amount of charge that a capacitor can store depends on the area between the plates, the distance between the plates and the dielectric constant of the material between. Capacitance measures the separation between the two conductive plates. Force can be either shear or normal force; shear altering the area of overlap between the plates and normal force affecting the plate separation. However, it is difficult to separate these two effects when trying to measure both shear and normal force at the same time. In both cases the change of force causes a change in capacitance which is then converted into voltage with the appropriate circuitry [1][10].

Capacitive touch sensing systems are of two types: self-capacitive, in which the object - e.g. human or robot finger - loads the sensor or increases the parasitic capacitance to ground; or mutual capacitive, in which the mutual coupling between two electrodes is altered. Self-capacitance is defined as the capacitive load, relative to circuit ground, that an electrode presents to the measurement system. Self-capacitance type systems are prone to false signals from unintended parasitic coupling. Mutual capacitive type touch sensors are more suitable for robotics applications, because the arrangement of sensor allows contact detection also for conductive objects (human fingers).

Capacitive sensors can be built almost in any shape or size, and either rigid or flexible. They can be made by micromachining silicon as well as by the conventional non-silicon technology. They can therefore be miniaturized, allowing construction of dense sensor arrays, as in many MEMS capacitive sensors, or can be made larger and suitable for a robot tool force sensor. With capacitive sensors, very high sensitivity in small packages can be achieved. They can be robust, endure millions of full-scale pressure cycles and withstand high peak loads, much more than a resistive sensor with similar sensitivity. Figure 13 illustrates SingleTact capacitive force sensor.

Figure 13. *SingleTact capacitive force sensor [15]*

Despite the advantages, capacitive load cells aren't appropriate for all applications. Sensor drift may cause problems when high accuracy for a long period is required. Temperature and humidity changes in the environment may cause problems. However, if the application requires a quick measurement with initial conditions reset frequently, and the application environment is steady, the capacitive technology is recommended.

When high spatial resolution is required, the size of capacitive pair must be reduced, and thus the sensors absolute capacitance will be small. In high spatial resolution measurements to maximize the change in capacitance – and thus the sensitivity - as the force is applied, a high permittivity dielectric material should be inserted between capacitor plates. Table 1 presents relative permittivity of different materials.

Table 1. *Relative permittivity of materials [16]*

Material	**Relative permittivity (εr)**
Vacuum	1
Water	30-88 (depending on temperature)
Air	1.00059
Glass	3.7 to10
PTFE (Teflon)	2.1
Polypropylene	2.2 to 2.36
Polymide	3.4
Polypropylene	2.2 to 2.36
Polystyrene	2.4 to 2.7
Titanium dioxide	86 to 173
Strontium titanate	310
Barium strontium titanate	500
Barium titanate	1250 to 10,000 (depending on temperature)
Conjugated polymers	1.8 to 100,00 (depending on type)
Calcium copper titanate	>250,00

3. EVALUATION OF TECHNOLOGIES

This chapter categorizes the technologies of Chapter 2, and analyzes their strengths and weaknesses. Then two of the technologies, best suited for the application of this thesis are selected and compared in detail. The evaluation of technologies, presented in table 2, is based on the following characteristics:

1. Dynamic range: The ratio between the smallest and the largest detectable force.
2. Spatial resolution: The spatial extent of a single sensing element. Many of these technologies are used in force sensing arrays where the spatial resolution gives the number of single sensing elements per given length or area.
3. Inherently dynamic: Sensor output decays to zero when constant load is applied.
4. Signal to noise ratio: The ratio between the signal power and the noise power.
5. Nonlinearity: The maximum deviation of true response to the best fit straight line
6. Hysteresis: The maximum difference between output readings when the same force is applied repeatedly under same conditions with force approaching from opposite directions.
7. Precision: The maximum difference between output readings when the same amount of force is applied repeatedly under same conditions.
8. Drift: The maximum shift of output while same force is applied by constant amount of time.
9. Resolution: The smallest reliable measurement the system can create.
10. Operating temperature: The temperature range where the output of the sensor remains in the operational limits assured by the manufacturer. Storage temperature may be different.
11. Temperature shift span: The maximum deviation of output as a function of temperature within the operating temperature.
12. Safe overload: The maximum amount of force which can be applied to the sensor safely so that it remains in specification, once the load returns to normal operating range.
13. Robustness: The capability of a system to resist change without altering its initial form.
14. Measurement interface: Specified technique for interfacing the sensor.
15. Complexness: The simplicity of electronics required to operate the sensor.
16. Power consumption: The electrical energy required to operate the sensor.

Table 2. *Evaluation of technologies*

Technology	Strength	Weakness
Resistive	- Wide dynamic range - Robust - Low cost - Easy to use	- Low signal to noise ratio - Low noise resistance - Power consumption - Small Gauge Factor
Piezoresistive	- Wide dynamic range - Low hysteresis - Low drift - Low cost	- Temperature sensitive - Lower robustness than fully resistive - Low overload tolerance
Piezoelectric	- Wide dynamic range - Durable - High sensitivity - Temperature and force sensing capability	- Inherently dynamic - Difficult to separate pyroelectric and piezoelectric effect - Good solutions are complex
Optical	- Wide dynamic range - Very high resolution - Immune to EMI - Processing electronics can be located away from the sensor	- Expensive - Low robustness – depending on elastomer design - Complex electronics - Power consumption
Ultrasonic	- Wide dynamic range - Good spatial resolution	- Complex electronics - Problems with acoustic coupling
Magnetic	- Wide dynamic range - Low hysteresis - Linear response - Robust	- Prone to stray fields and noise - Complex electronics required
Capacitive	- Wide dynamic range - Low cost - High sensitivity - High signal to noise ratio - Robust	- Complex electronics - Capacitive crosstalk - Limited spatial resolution - Some dielectrics are temperature sensitive

3.1 Comparison of commercial sensors

Table 3 presented the sensors of two most attractive technologies, resistive and capacitive, which dominate in the tactile pressure and force sensing sector. Although other technologies have their advantages, they do not necessarily have commercial solutions in tactile load cell and pressure sensing applications. There is no single reason for this, some are inherently dynamic and as such not suitable for these purposes, or engineers generally prefer to use sensors as simple, inexpensive and reliable as possible.

The first comparison is for load cells, which are constructed for larger forces and therefore are also very robust. Futek LSB200, which is a resistive strain gauge with S-beam mechanics [7], is to be compared with iLoad mini capacitive load cell from Loadstar with button mechanics [14]. The second comparison is in the foil sensor category, which are very light, thin and generally cheap options: FlexiForce A101-A piezoresistive pressure sensor from Tekscsan [8] is compared with a capacitive pressure sensor from SingleTact [15]. The cell value is marked as N/A if sensor manufacturer did not inform some of the attributes in the datasheet.

Table 3. *Resistive and capacitive sensor comparison*

	Futek LSB200	**iLoad mini**	**FlexiForce A101-A**	**SingleTact**
PERFORMANCE				
Nonlinearity	± 0.1%	± 1%	< ± 3%	< 2.0%
Hysteresis	± 0.1%	± 1%	< 4.5 %	< 4.0%
Accuracy	± 0.05%	± 1%	< ± 2.5%	< 1.0%
Drift	N/A	± 0.03% (in 20 min)	N/A	< 2% per log. time scale
Resolution	N/A	N/A	N/A	< 0.2% of Full Scale
ELECTRICAL				
Measurement interface	Wheatstone bridge	DQ-4000 Frequency to USB Interface	Resistance measurement with multimeter or similar electronics	I2C (100kHz), 10-bit resolution
MECHANICAL				
Safe Overload	1000 %	150%	N/A	300 %
Material	Aluminum	Aluminium	Polyester	Polyimide
TEMPERATURE				
Operating Temperature	-50°C to 93°C	10°C to 40°C	-40°C to 60°C	-40°C to 85°C
Temperature Shift Span	0.036%°C	±0.05 %°C	N/A	0.2% /°C

3.2 Motivation for the capacitive load cell design

In this thesis, the capacitive technology for sensor implementation was chosen. This chapter presents the motivation for the capacitive sensor design, and the reasons - in addition to the preferred attributes of low price, high sensitivity, small size, simple to use and robustness - why this technology approach was chosen. The decisive factor was the mechanical structure, in which the sensor and its mechanism was intended to be implemented. The mechanical structure is further described in Chapter 4.

Capacitive pair was formed with two conductive plates with air as a dielectric material between the plates. Measurement circuitry for capacitance was designed with inexpensive components. The remaining design task was to design a sensitive and adjustable mechanism to link the change in force to change in capacitance, by altering the distance between conductive plates. This led to the sensor design presented in Figure 14.

The sensitivity of capacitive sensor can be tuned to match the application. If there is a need for high sensitivity, the load-free gap between the plates is be minimized. This is because the capacitance is inversely proportional to the gap between the electrodes, see Eq. (3) and thus the sensitivity drops significantly with larger gaps [1]. The distance between the conductive pair in Figure 14 can be adjusted between 0.1 and 6mm. In the present design, the two small overlapping discs have a radius $r_1 = 3\,mm$ and a center hole radius $r_2 = 1mm$. The total area of overlap is

$$A = \pi {r_1}^2 - \pi {r_2}^2 = 25{,}13\,mm^2 \tag{4}$$

The separation of the discs with no load is $d_1 = 1mm$ and only air is between the discs. Then the load-free capacitance C_1 of the system is

$$C_1 = \frac{\varepsilon A}{d_1} = \frac{1.00059 * 8.854 * 10^{-12}\frac{F}{m} * 25{,}13 * 10^{-6}m^2}{1 * 10^{-3}m} = 2{,}23 * 10^{-13}F \approx 0{,}22pF$$

However, when the sensor is fully loaded, the gap between conductive plates decreases to its minimum which is approximately $d_2 \approx 0.1mm$. This approximation takes into account the tolerances in manufacturing and assembly. Therefore, it is highly unlikely that the plates would never be in contact. By these assumptions, the capacitance of the sensor during full load is

$$C_2 = \frac{\varepsilon A}{d_2} = \frac{1.00059 * 8.854 * 10^{-12}\frac{F}{m} * 25{,}13 * 10^{-6}m^2}{0{,}1 * 10^{-3}m} = 2{,}23 * 10^{-12}F \approx 2{,}2pF$$

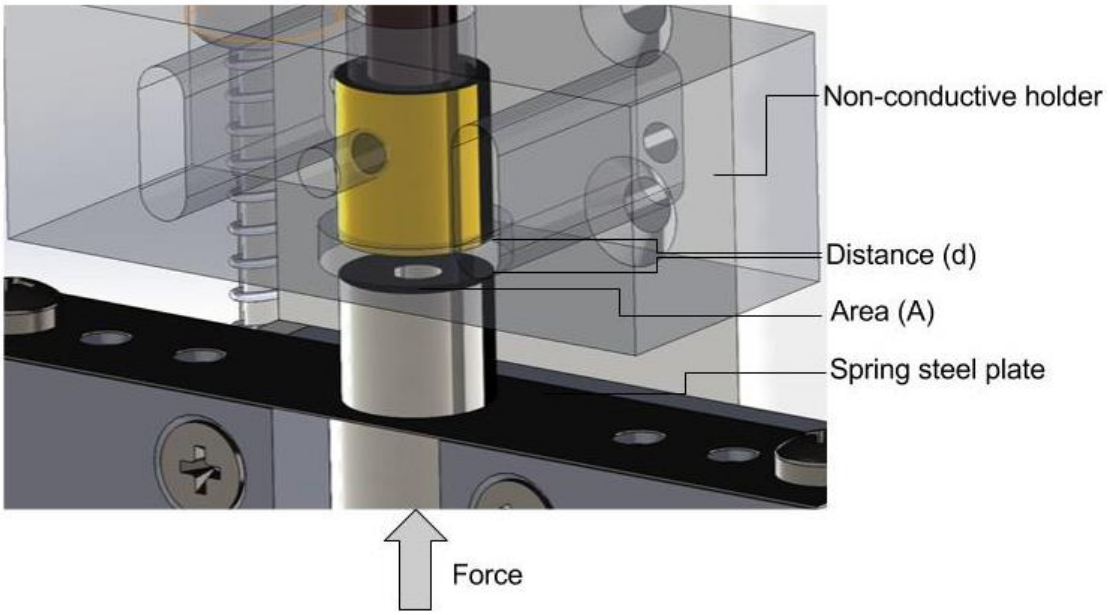

Figure 14. *Illustration of the designed sensor*

The percentage increase from C_1 to C_2 is $(2{,}2pF - 0{,}22pF)/0{,}22pF * 100 = 900\%$. This means that capacitive measurement is a highly sensitive technology and will provide high signal to noise ratio for near full load measurements.

The measurement electronics for changes in capacitance or in resistance are very similar. However, instead of measuring change in analog DC voltages in a magnitude of micro to millivolt range like in strain gauges, change in capacitance is measured in a discharge frequency. Capacitive sensor converts the physical input signal to the electrical output signal in two steps: firstly, by transducing a physical input into a change of electric capacitance; then, measuring and converting the capacitive signal into an electric output signal. By converting the capacitance to a square wave with an amplitude of 5 volts, meaning that the signal is inherently digital and immune to noise after the capacitance to frequency conversion. Digital input transitions are possible to read with a digital input module available for most of the common micro-processors and programmable logic controllers. The frequency response of designed sensor can be seen in Figure 15.

Signal being immune to noise, provides vast advantage as the sensor location is in the end effector of a robot, which is often driven by three or more motors. This means that measured signal needs to be wired all the way through the robot's energy chain to the PLC or microprocessor and it will run in parallel to noisy control cables. In many cases this means at least a few meters of wire which is prone to different sources of noise.

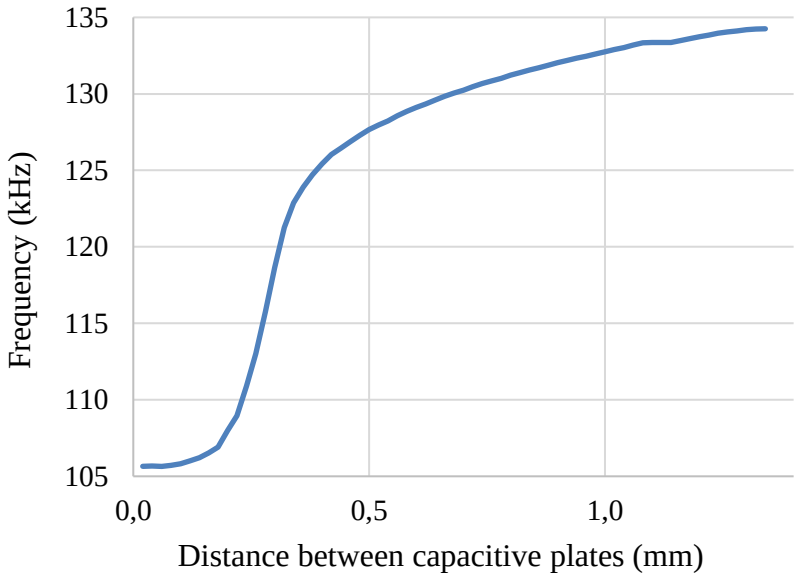

Figure 15. *Frequency response of the designed sensor*

3.3 Comparison to resistive load cell operation

A load cell can be made for example the shape of a cantilever beam, pancake or an s-beam with one or several strain gauges attached to the mechanics. When a force is applied to a load cell, it deflects by a few thousands of a millimeter in response to the applied force and generates strain on the strain gauges. Strain affects to the resistivity of a strain gauge. For a 350 Ohm strain gauge the change in resistance during full range of motion can be 0.7 Ohms, resulting only in a $(350\Omega - 349.3\Omega)/350\Omega * 100 =$ 0.2% change in the resistance.

The change in resistance is often measured with a balanced Wheatstone bridge illustrated in Figure 16. Typical Wheatstone bridge converts this full range of motion into an output change of 20 millivolts, which needs to be converted into 5000 discrete levels if 0.02% accuracy is required. In order to achieve this magnitude of accuracy, the input voltage and the output signal resolving must be carefully conditioned. At least 2 mV resolution with several times per second measurement is required. This means that, for example, a response rate of 100 Hz needs a high-quality analog-to-digital converter.

There is a limit on how small the strains can be measured. As the application mechanics becomes smaller, the strains become smaller too. To achieve a reasonable resistivity change, the mechanical deflections need to be increased. This means the sensor becoming less robust and more delicate, leading to a need for repeated calibrations, or in the worst case, sensor being damaged often [14].

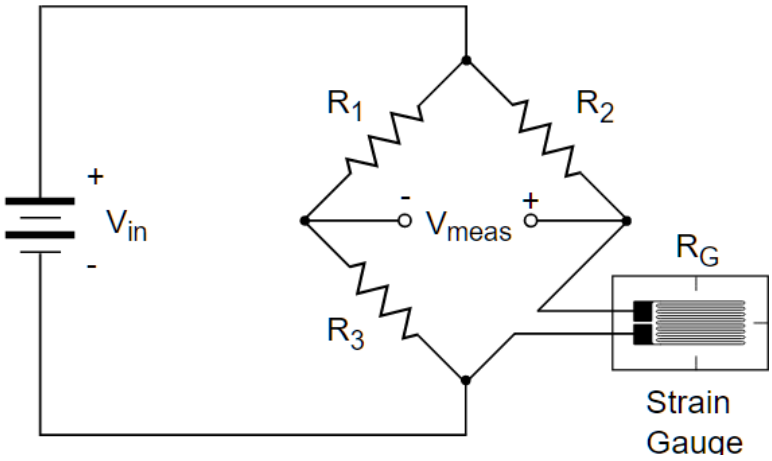

Figure 16. *Illustration of Wheatstone bridge with strain gauge [17]*

3.4 Piezoelectric sensor comparison

The disadvantage of piezoelectric sensors is that with them a genuinely static measurement is not possible. A static force in a piezoelectric material results in a fixed amount of charge. This means that in conventional electronics, with imperfect insulating materials and due to internal sensor resistance electrons are lost and the signal decays. At higher temperatures, the internal resistance and sensitivity deteriorate. Piezoelectric sensors have their strengths and are best used in fast changing measurements and processes, but for the transient nature, manufacturers do not implement piezoelectric technology to load cells.

3.5 Conclusions of sensor implementation

Capacitive sensors can be made in various forms and the manufacturing process of a conductive pair is simple and solutions are robust. Mechanism, which uses resistive strain gauge would require a smooth, clean surface on which the strain gauge is glued with carefully chosen adhesive. Although a readymade load cell from a sensor manufacturer can be purchased, it requires mechanical design to implement the load cell to the target mechanics. High sensitivity was one of the core criteria defined for the application in this thesis. As described in this Chapter, capacitive technology provides a faster and more sensitive response to change in force. As seen in Figure 15, the sensor's frequency response is from 134 to 106 kHz during its 1.32mm movement range, meaning high sensitivity and fast frequency response.

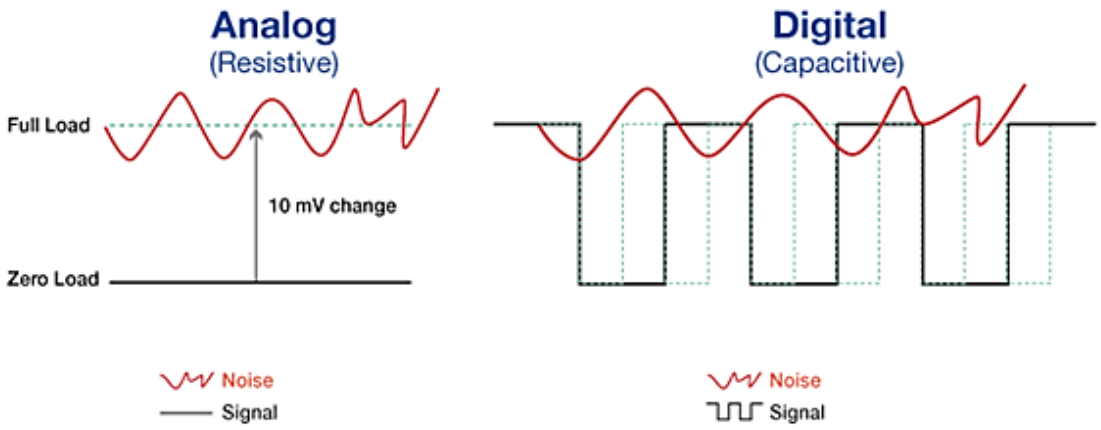

Figure 17. *Signal levels with noise component [14]*

The measurement electronics for capacitance can be more complex than those of a strain gauge, but the capacitance measurement does not require a calibrated power supply as resistive strain gauge with balanced Wheatstone bridge does. In addition, the capacitive measurement is practically immune to noise, assuming that the sensor element is protected from stray capacitance. Figure 17 illustrates the noise component with both resistive and capacitive signal levels. Even random noise in 10mV level can cause huge problems when the measured payload is also in the same range, whereas with capacitive measurement this is insignificant.

The cost of one piece of designed mechanics consisting of the capacitive pair and electronics is roughly 150€. The cost of resistive S-beam strain gauge LSB200 from Futek is around 500€. When produced in volumes, the cost of capacitive sensor can be significantly lower as manufacturing costs per unit decreases when production volumes increase. The resistive strain gauge on the other hand needs to be still outsourced and even larger order quantities will not affect unit price significantly. Capacitive force sensing technology offers a good combination of high sensitivity, small size, low cost and robustness therefore achieving all the preferred attributes for a good tactile force sensor.

4. MECHANICAL DESIGN

Various mechanical designs can be used in the development of a tactile force sensor. The design in this thesis was application driven: the selection of technology and the decisions made in mechanical design were driven by the existing One Finger mechanics, system robustness and keeping the cost of the solution low enough. The design process was iterative as the understanding of the system grew through time. The presented design is the third, hopefully final version. Rapid prototyping methods were utilized and machined parts were first 3D-printed. This method provided good results, fast feedback from the design and no changes needed to be done after first fully machined assembly.

4.1 One Finger mechanical design

One Finger is a product of Optofidelity. It is a simple robot end effector and is used for touch screen testing. One Finger was the base for the new sensor mechanics because it offers a generic attachment plate and in ideal case, the new design could be retrofitted to every One Finger ever sold. One Finger mechanical design consists of a robot-to-tool adapter on which the tool is connected to the robot wrist, an attachment plate for the adapter, a baseplate for sliding block, sliding block which is composed of a linear slide rail and linear ball bearings, a mount for the finger shaft, and a finger and spring system to adjust the displacement return force.

4.2 New mechanical design

The new mechanical design has the same components as One Finger . A new type of attachment part, called spring sheet mount, replaces the mount for finger shaft. In addition to this, the finger shaft has been divided in three parts, which are mounted together with M5 threads. This assembly holds the two changeable spring steel plates together and thickness of the spring steel determines the force response of the sensor. Solid 5 mm magnet in finger is replaced by a ring magnet, which allows the change of fingers automatically and gives the possibility to insert an optical fiber through the finger. Located at the top is the capacitive pair for which the tool baseplate is used as electrical ground. The counterpart of the capacitive element is isolated from the baseplate by a 3D-printed mount made of polylactic acid (PLA). This mount is also used as capacitance-to-frequency printed circuit board (PCB) holder. A cover made of 2 mm thick steel plate is placed to protect the mechanics, the electronics and the capacitive pair. The exploded view of the designed mechanics is shown in Figure 18.

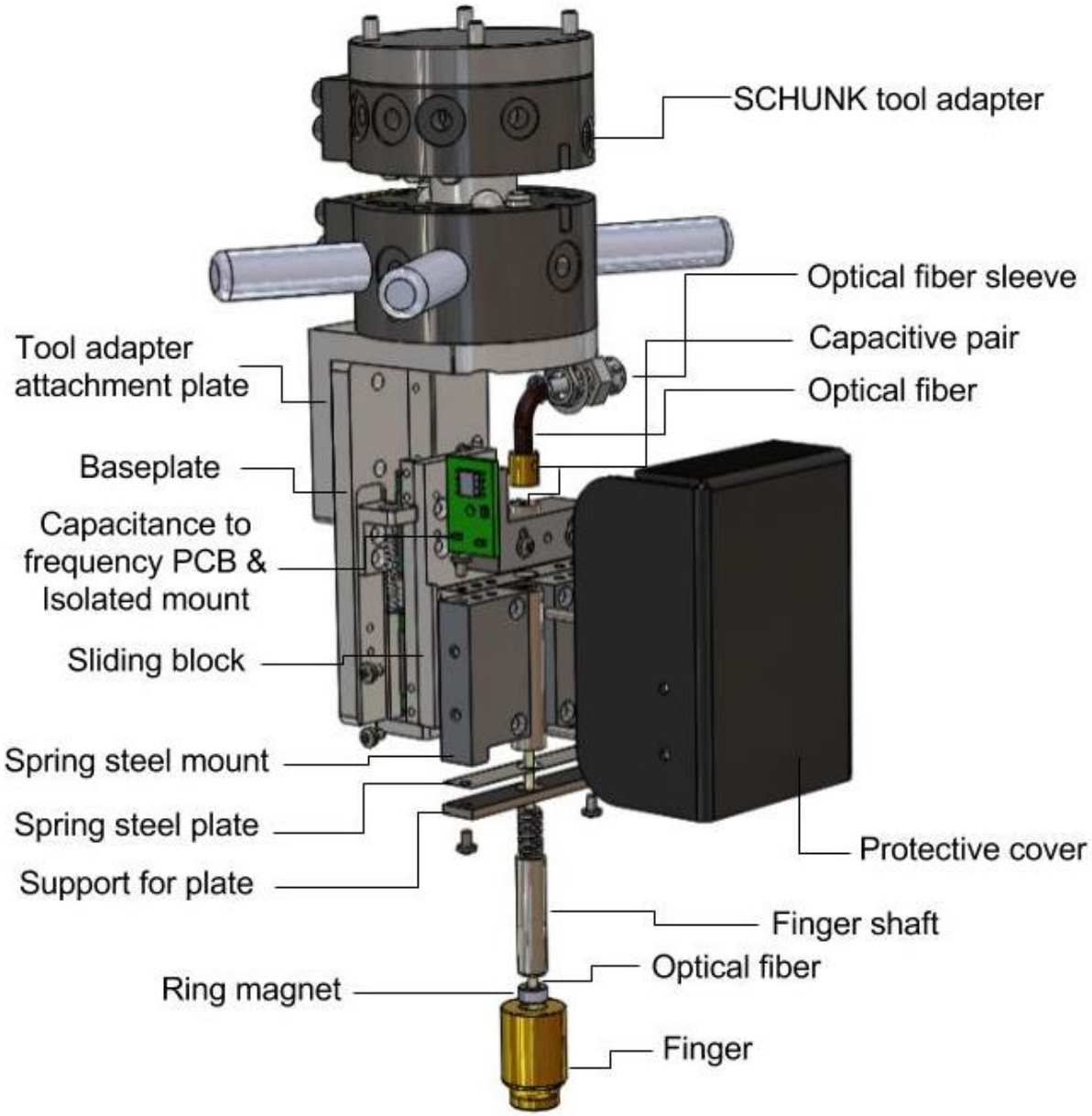

Figure 18. *Exploded view of designed tool mechanics*

The core component related to the sensor force response is the 1.4310 grade stainless spring steel wire [18]. The sensor mechanics consists of two changeable spring steel sheet flexures the thickness of which can be adjusted depending on the needed force response. The sensor mechanics define the maximum bending range for the spring sheet from the middle section. This bend range is equal to the initial distance between the capacitor plates and it can be adjusted from 0.1 to 6mm. The force response of the graded spring sheet is highly linear as shown in Figure 19 where the system force response with 0.1mm thick spring sheets is measured. The linear properties of graded stainless spring sheets turned out to be important later when the force-to-capacitance relation is measured and linear interpolation is applied.

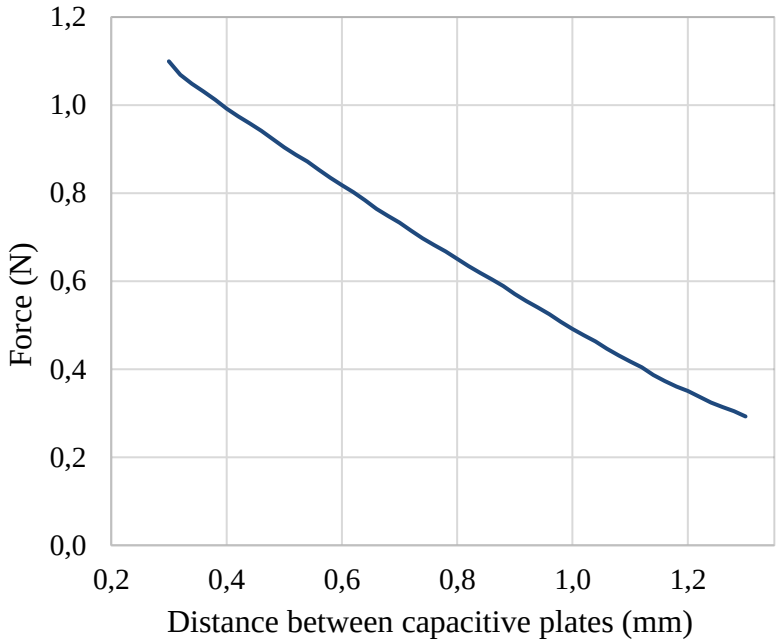

Figure 19. *Force response of designed sensor with 0.1mm spring sheet*

A fair amount of design time was spent in inventing a solution to deliver optical fiber through the finger and the moving parts without interfering the fine mechanics or the measurement process, which turned out to be a real challenge. Due to characteristics of capacitive sensor, even a small movement in finger mechanics produces a high response in capacitance. This small movement can be accurately aligned therefore the delivering and the receiving fiber ends can hold their concentric position during the full range of motion. Although the fiber ends are in physical contact at the end position, they need to be thoroughly polished to prevent excessive loss in light amplitude. Figure 20 shows a cross-sectional view of the construction where the fiber is highlighted in red and the gap is slightly exaggerated.

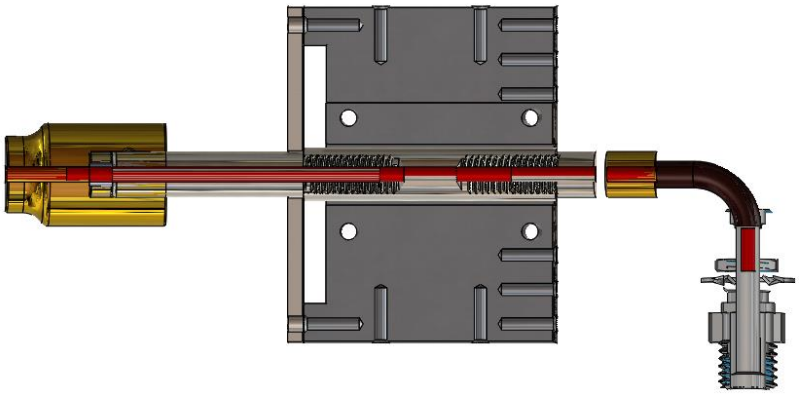

Figure 20. *Section view of fiber inserted through the sensor mechanics*

5. ELECTRICAL DESIGN

5.1 One Finger electrical design

One Finger is equipped with two optical trigger circuit boards. One of the triggers positions robot on z-direction with a calibration pad. The other trigger, the upper optical gate is the end limit switch for the tool's z-axis movement, triggering an emergency stop: the movement is halted, if the robot tries to move too deep on the z-axis and is in danger of damaging itself or the device under test.

The calibration pad is a simple PCB with three contact pads and a resistor. Robot tool is usually grounded to potential of 0 VDC. When some of the contact pads is touched with the tool, a galvanic connection between the finger and the pad is formed. This causes change of potential in the calibration pad output and this information triggers a start of a timer. As the speed of a robot is assumed to remain constant and the robot is moving in the positive direction on the z-axis, it eventually triggers the first optical gate. This can be used as a signal to stop the timer. When distance travelled from calibration pad contact to optical gate is always the same and robot speed remains constant, the moment of touch can be calculated afterwards.

5.2 New electrical design

The idea in new electronic design was to rely on One Finger electronics in normal operation of the robot and install new electronics next to it. In addition of the two optical gate boards, a capacitance-to-frequency converter circuit board is used. This board is designed around a 555-timer IC which is an integrated chip used in a various timer, pulse generation and oscillator applications, providing time delays, an oscillator functionality, or a flip-flop circuit. The 555-timer was first introduced in 1972 and is still widely used due to its low price, ease of use, and stability. Actually, it is the most popular integrated circuit ever manufactured [19][20].

As shown in Figure 21, the basic blocks of the 555-timer are:

- Trio of identical resistors
- Two voltage comparators
- A flip-flop
- A BJT switch at Q_0

The resistances set the comparator thresholds at $V_{TH} = (2/3)V_{CC}$ and $V_{TL} = (1/3)V_{CC}$, as seen in Figure 21 between the 5 kΩ resistors. The state of the flip-flop is controlled by the comparators in the following way:

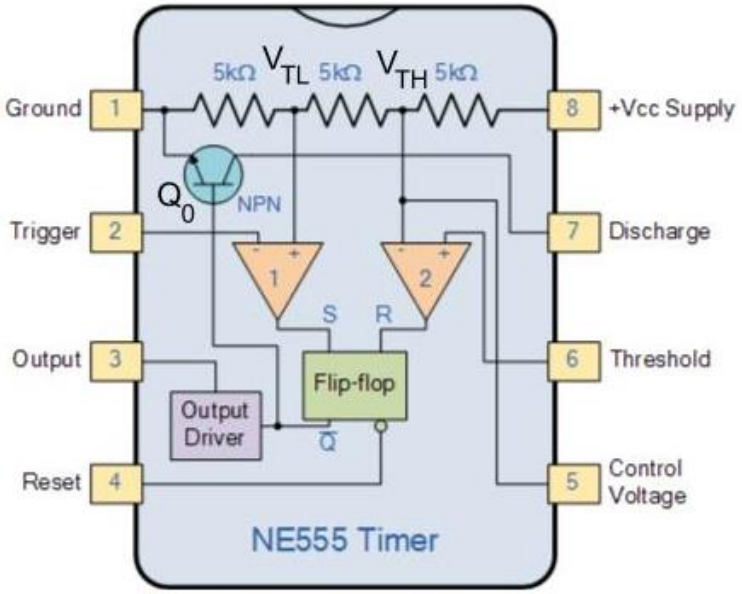

Figure 21. *Block diagram of 555-timer IC [21]*

When the voltage at the $Trigger$ input drops below V_{TL}, comparator 1 fires and sets the flip-flop, forcing $\bar{Q}$ low. With low voltage applied to Q_0 base it is in cutoff. Whenever the voltage at the $Threshold$ input rises above V_{TH}, comparator 2 fires and clears the flip-flop, forcing $\bar{Q}$ high. Q_0 is now on with a high voltage applied to its base. The flip-flop includes a $Reset$ input to force Q_0 on, regardless of the conditions at the inputs of the comparators [19].

The 555's three main operating modes are astable, monostable and bistable. An astable circuit has no stable state and the output constantly switches between high and low, producing as an output a square wave. Astable circuit can be used, for example, to flash lights, to generate pulses or tones, and in logic clocks. Pulse generation capability is applied in this work, where the 555-timer is used as an ADC converter, converting the analog input to a square wave output.

Monostable circuit produces one pulse of a preset length in response to a trigger input such as a button. The output of the circuit stays in the low state until there is a trigger input. This type of circuit can be used in a push to operate systems.

Bistable mode, also known as the Schmitt Trigger, has two stable states of high and low. Taking the trigger input low makes the output of the circuit go into the high state. Taking the Reset input low makes the output of the circuit go into the low state.

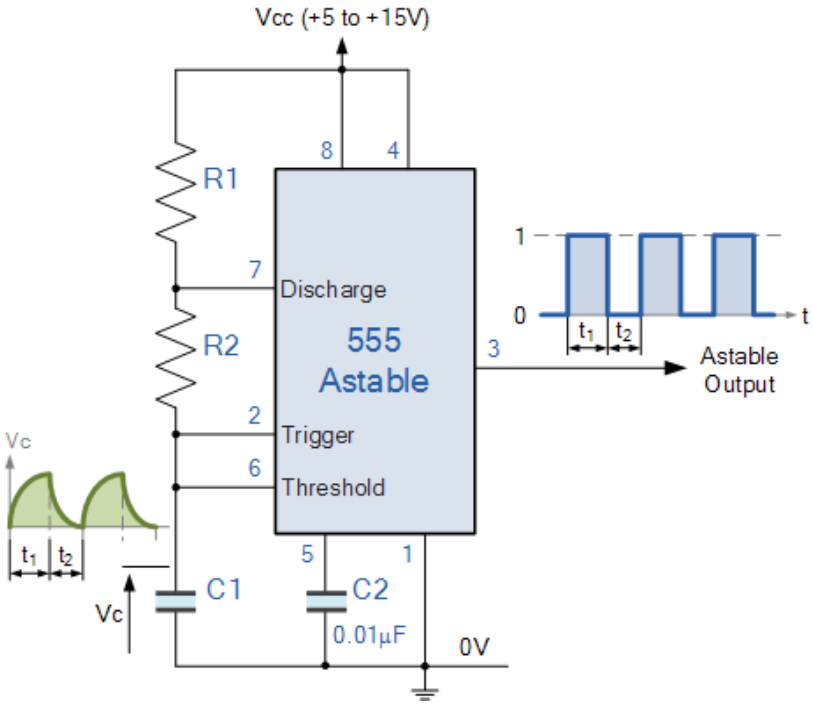

Figure 22. *Astable circuit where C1 is capacitance variable [21]*

The circuit in astable mode is illustrated in Figure 22. The logic of the circuit is as follows. Pins 2 and 6 are connected, allowing the circuit to operate as a free running oscillator and to re-trigger itself on every cycle. Capacitor $C1$ charges up through both timing resistors $R1$ and $R2$ during each cycle, but discharges itself only through resistor $R2$, as the other side of it is connected to the discharge terminal at pin 7. Then the capacitor charges up to V_{TH}, the upper comparator limit and discharges itself down to V_{TL}, the lower comparator limit. This results in an output of square wave of which voltage level is equal to $V_{cc}- 1.5V$ and of which output duty cycle is determined by the capacitor and resistors combinations. To prevent power supply noise from causing false triggering, a 10 nF bypass capacitor between pin 5 and ground is used. The timing accuracy of the 555 astable circuit approaches 1% with temperature stability of 0.005%/°C and power supply stability of 0.05%/V [19][21].

Below are the equations for individual times required to complete one charge and discharge cycle of the output is therefore given in equations 4 and 5, where t_1 is time on and t_2 is time off.

$$t_1 = \ln(2) * (R_1 + R_2) * C \tag{4}$$

$$t_2 = \ln(2) * R_2 * C \tag{5}$$

The duration of one full timing cycle is the sum of the two individual times seen in equation 6 which the capacitor takes to charge and discharge:

$$T = t_1 + t_2 = \ln(2) * (R_1 + R_2) * C + \ln(2) * R_2 * C \quad (6)$$

The oscillation frequency is the inverse of the cycle time and the duty cycle is the ratio of the on time and cycle time:

$$f = \frac{1}{T} = \frac{1}{\ln(2)*(R_1+R_2)*C+\ln(2)*R_2*C} \quad (7)$$

$$D(\%) = 100 * \frac{R1+R2}{R1+2R2} \quad (8)$$

As presented in Chapter 3, the capacitance of the designed sensor varies in between 0.67 – 6.7 pF. Based on the circuit time expressions above, the output frequency is defined by the RC circuit. In this circuit, the resistors are the main variable as the change in sensor capacitance can be considered constant. By a choice of the resistors, the output frequency of the circuit can be trimmed to desired level. The EL5101 incremental encoder unit was used to calculate frequency from the sensor circuitry. It can sample pulses up to 1 MHz and so it defines the maximum output frequency and the values of resistors. The circuitry output was trimmed below 1 MHz, according to Eq. 7. The final design resulted in a frequency of 134 Hz at 0.67 pF capacitance. The EL5101 incremental encoder is mainly used with differential encoders, but it can be used in single ended mode. To ensure the stability in the single ended mode, the input was connected to the encoder terminal A+ and A- was grounded.

6. MEASUREMENT SYSTEM

This chapter presents the measurement system and evaluates possible sources of measurement deviation and system error. The measurement system consists of OF-400 robot, the designed robot tool, EtherCAT PLC measurement module, Kern PCB scale and Advantech ARK-1134 embedded PC [22] on which the Twincat 3 is the development environment and control program is run. System setup can be seen in Figure 23.

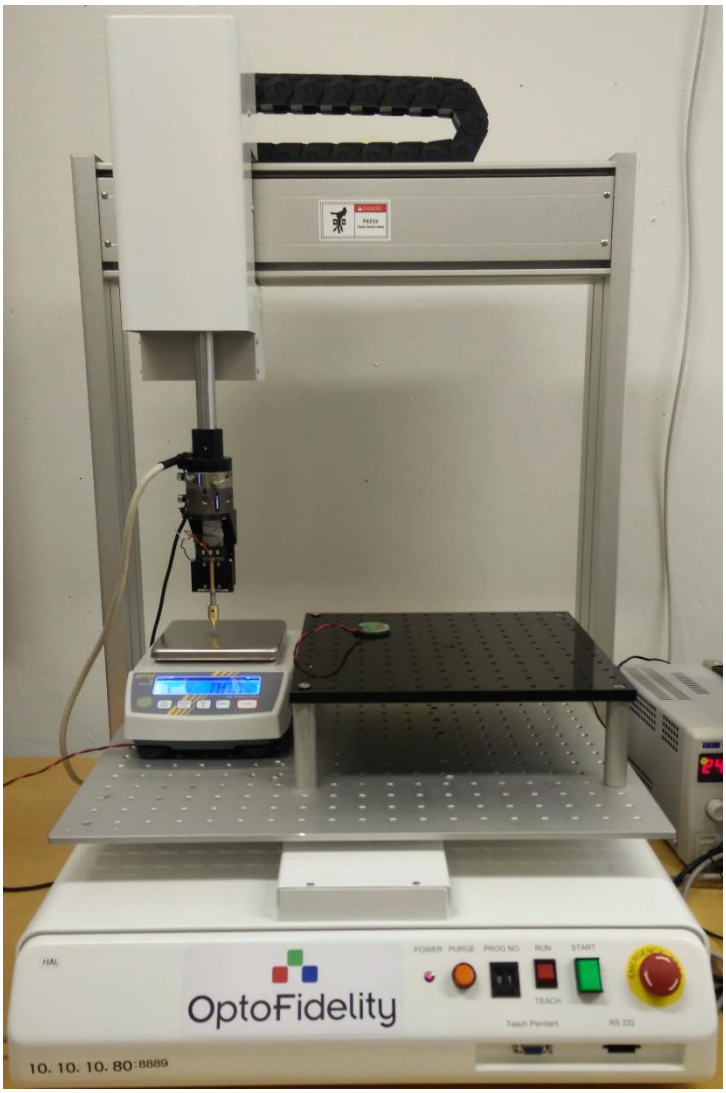

Figure 23. *OF-400 Robot and measurement setup*

6.1 Hardware configuration

Measurements are done by connecting the designed tool to the wrist of OF-400 cartesian robot. OF-400 robot is a four-axis step motor driven desktop robot, designed primarily for touch testing of smart devices. The robot is controlled by Touch and Test server and the test programs are done with Sequence Generator. Both Touch and Test and Sequence Generator are Optofidelity software products designed for automated smart device testing. Figure 24 presents the designed tool without cover and an illustration how the hardware is connected.

Beckhoff PLC system was chosen for developing the measurement environment. Beckhoff offers a wide variety of hardware components for signal processing and is relatively inexpensive. The main program runs on Advantech ARK PC, it has a four-core processor of which one core is dedicated for real time applications. Measurements are read by a separate module closer to robot. This separate module consists of a Beckhoff EK1100 EtherCAT coupler [23], an EL5101 incremental encoder [24], an EL1094 negative switching input terminal [25], and an EL2008 digital output terminal [26]. Beckhoff modules are connected, and the EtherCAT module communicates with ARK PC via EtherCAT fieldbus. By this configuration, the system can be categorized as a distributed automation system.

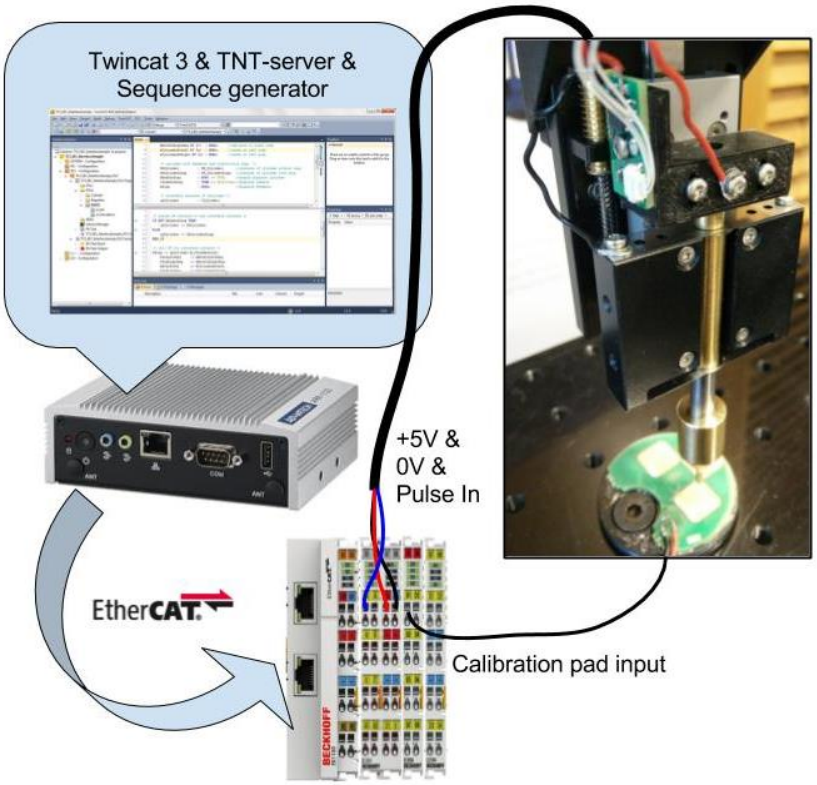

Figure 24. *Hardware connections*

6.2 Measured signal propagation

The change in the capacitance causes the 555-timer circuit to change its output frequency. The pulses generated by 555-timer circuit are transferred to EL5101 incremental encoder. The encoder counts the pulses and saves the sum to a variable. This variable can be read with PLC on each program cycle. The difference in total pulses between two consecutive program cycles is then calculated and the derivate value is saved to another variable. This new variable is then filtered with a geometric moving average (GMA) filter in the PLC program and the result of this filtered value is used in touch sensing algorithm. GMA is a common method to filter out signals with high sample rate in signal processing.

Excessive shot noise was detected during the PLC program development and regardless of several consulting opinions, the source of it was not discovered easily. The source turned out to be the processor load caused by the Twincat oscilloscope during the measurement process, i.e. the measurement software itself caused the noise. This was solved by reducing the program cycle time from 0.1 ms to 0.2 ms.

6.3 Program

The program for the PLC is developed with Beckhoff Twincat 3. It is written according to the IEC61131-3 standard, that defines ladder diagrams, function block diagrams, structured text, instruction lists, and sequential function charts. In this thesis only structured text and function block diagrams were used. Implementation has one main program, which contains six networks. Each network contains function blocks, which are mainly self-programmed with structured text. This divides the main program to smaller modules so that the managing of a larger program is more straightforward and visually easier to interpret.

The first network contains a pulse counter function block, which takes the total pulse value from pulse encoder input and calculates the differential between two consecutive program cycles. This is the core measurement and the most important value for touch sensing algorithm used in network 4.

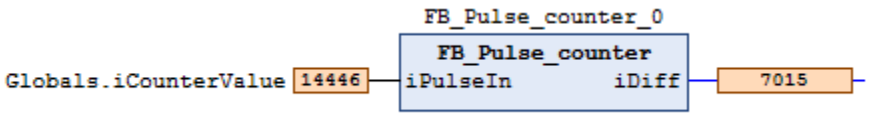

Figure 25. *Pulse counter function block*

In the second network a geometric moving average filter takes input of the pulse count difference from the first network, alpha as predefined filter value, reset information, and gives as an output the filtered pulse count difference.

The geometric moving average is a type of infinite impulse response filter. The GMA is used to smooth out short-term fluctuations and highlight long-term trends or cycles. Mathematically, a moving average is a convolution and thus a low-pass filter in signal processing. To put it simply, the GMA smooths the data [27]. The GMA filter is implemented as

$$S_t = \alpha * Y_T + (1 - \alpha) * S_{T-1} \tag{7}$$

Here S_t is the new filtered value at time t, α is the predefined filter parameter between 0 and 1, Y_T is current input value at time t and S_{T-1} is previous filtered value at time $t - 1$. For example, in Figure 26, where alpha value of 0.1 is used, means that every program cycle a new filtered value is a sum of 10 percent of the current input value and 90 percent of previous estimated value.

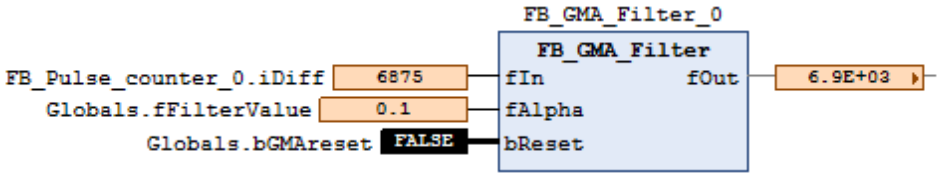

Figure 26. *GMA filter function block*

The third network contains a calibration function block which takes as an input the GMA filter output and, when requested to, gives a calibrated signal value which is later used as trigger value for the touch sensing algorithm. It also produces a logic output for successful calibration as seen in Figure 27. The calibration value is determined by measuring the current noise value for five seconds and the lowest recorder value is then saved in a variable. Experience has shown that this lowest recorded value needs to be compensated, because otherwise it is unnecessary low for touch trigger value. As found by trial and error, a 0.1 percent addition to current lowest value is a good compensation.

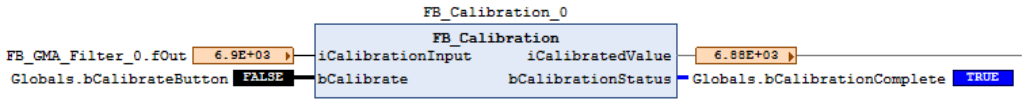

Figure 27. *Calibration function block*

The fourth network is the touch sensing algorithm. It combines the information from the previous networks and provides a Boolean output if touch has been detected or not. This output is linked to the digital output module which in turn connects to the robot. As seen in Figure 28, the touch trigger function block takes the following inputs: unfiltered difference value of pulse count, filtered value of pulse count, and the calibration level.

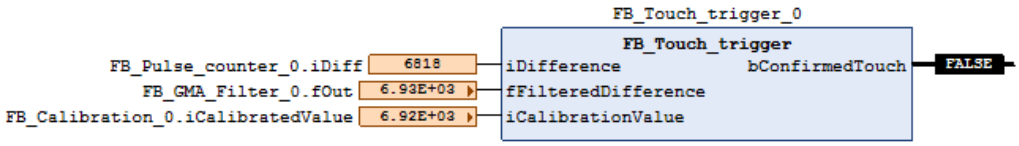

Figure 28. *Touch trigger function block*

This algorithm must be able to respond with a delay less than 1.5 ms and still be able to give reliable information. If trimmed too sensitive, pseudo-touch events will be registered whereas if trimmed too loose, unnecessary delay in measurement is caused. Through trial and error the following algorithm was developed. In every program cycle the filtered measurement value is compared to the calibrated value. If it exceeds the calibrated value, a touch is registered. The total measurement time is 1 millisecond when the program cycle time is 0.2 millisecond.

```
(*Touch trigger algorithm*)

IF iMeasurementRev <= 5 THEN        // Measuring 5 program cycles
      IF fFilteredDifference <= iCalibrationValue THEN
      // Compare each cycle value to calibration value
            iConfirmedMeasurement := iConfirmedMeasurement + 1;
      END_IF
      iMeasurementRev := iMeasurementRev + 1;
END_IF

IF iMeasurementRev >= 5 THEN
// if 5 or more measurements are below calibration value, touch is registered.
      IF iConfirmedMeasurement >= 3 THEN
      bConfirmedTouch := TRUE;
      ELSE
            bConfirmedTouch := FALSE;
      END_IF
      iMeasurementRev := 1;   //After 5 program cycles, reset variables
      iConfirmedMeasurement := 0;
END_IF
```

The fifth network, see Figure 29, is the reaction time calculator, which has an important role in filtering out the switch oscillation of contact between the calibration pad and the finger. This function block takes as an input the output of the touch trigger algorithm output and compares it to the real world touch event obtained from the physical contact between the finger and the calibration pad.

System reaction time is an important attribute as it represents the resolution of the system in touch sensing. When the robot begins its tap test cycle, it approaches the calibration pad and sets the tool above the calibration pad. Then the robot begins the tap sequence and moves its z-axis up and down repeatedly until the predetermined amount of cycles is completed.

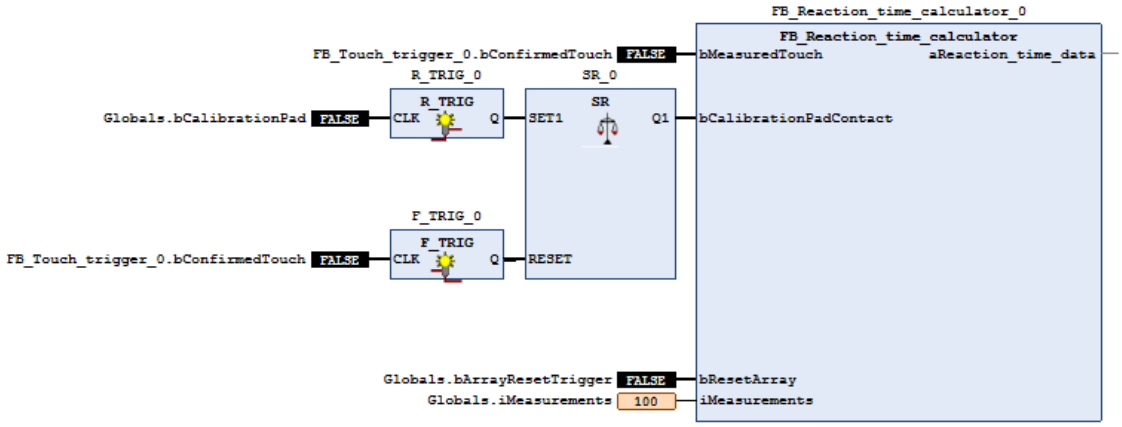

Figure 29. *Reaction time network*

On each cycle as the finger contacts the calibration pad a galvanic connection is formed. This acts as a trigger for the timer, which is stopped when the touch sensing algorithm senses the touch as well. The time between these events is the system reaction time. Figure 30 shows the oscilloscope view of the event, where the calibration pad input is in green and the touch sensing algorithm output in red. Calculations and timers are based on PLC real time engine and the program cycle time of 0.2 milliseconds, running on a dedicated real-time core on Advantech PC.

When the galvanic connection is formed, it triggers an input of EL1094 terminal. This terminal block was specifically chosen as it has a fast input filter of 10 microseconds. A significant amount of the switch oscillation can be detected during the first 7 milliseconds before it stabilizes. Although the input oscillates, the system cannot predict future. The first time when the input is activated, the timer is triggered. Significantly better results could be achieved if the timer was triggered when the galvanic connection has stabilized.

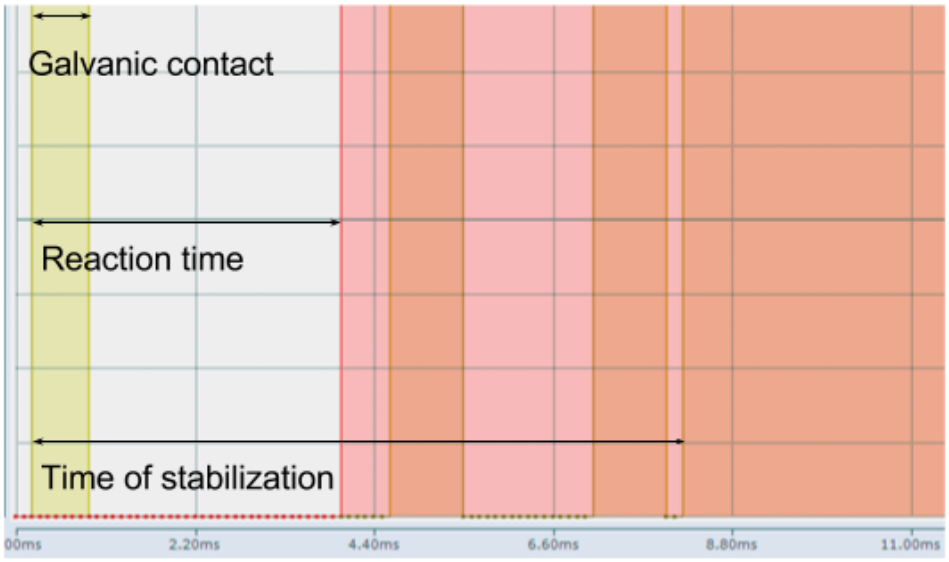

Figure 30. *Oscilloscope view of contact oscillation*

In the final network, see Figure 31, is the force function block which generates force output from the frequency input by linear interpolation. This function block takes as an input the spring sheet steel thickness and the filtered frequency value calculated by the incremental encoder module.

The linear interpolation program has a predefined table of measured frequency as a function of force. By this table and the information of thickness of the spring steel sheet the program produces output in grams. In mathematics, linear interpolation is a method of curve fitting by using lines to construct new data points within the range of a discrete set of known data points [28].

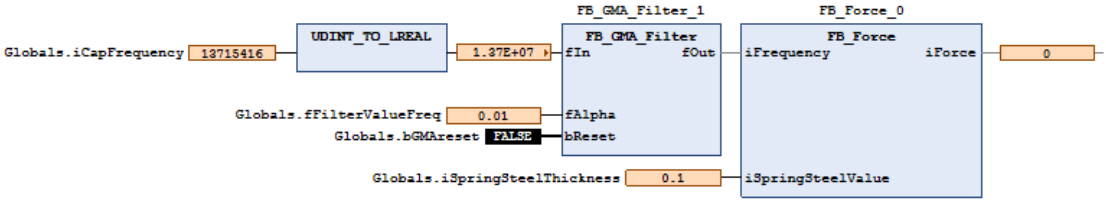

Figure 31. *Force network*

7. SENSOR CHARACTERISTICS AND RESULTS

7.1 Anti-aliasing

The Nyquist criterion dictates that all signals must be bandlimited to less than a half of the sampling rate of the system. Many of the signals are inherently limited by the spectrum and constitute no problems. If the signal has power above half the sampling rate, an analog low pass filter must be placed before the data acquisition system [29]. The basic frequency spectrum of the measurement in this thesis varies from 135 kHz to 105 kHz. Although the signal frequency band is at high frequencies, aliasing will not cause problems as the measurement system has an integrator in a form of incremental encoder module. This module can sample pulses up to 1 MHz and can give the total pulse count for PLC at every program cycle.

7.2 Noise and stability

Any unwanted disturbance that interferes with measured signal can be referred to as noise. Depending on its origin, noise can be classified as external or internal noise. External noise is caused by any unwanted interaction between the circuit and the outside. Sometimes even other parts of the circuit itself can interfere with itself.

External noise can be electric, magnetic, electromagnetic or electromechanical. Electric and magnetic noise affects through parasitic capacitances and mutual inductances between circuits. Electromagnetic interference originates from the fact that every wire and trace acts as an antenna. External noise interferes with a measurement system or its circuit via ground and power-supply busses. Precautions, such as filtering, decoupling, guarding, shielding, physical reorientation of components, low noise power supplies and ground-loop eliminations can be applied to reduce this noise. Internal noise will remain even if all external noise is removed. This form of noise is random by nature and due to phenomena, such as thermal agitation of electrons in resistors and random generation and recombination of electron-hole pairs in semiconductors.

Sources of noise can be for example thermal noise, shot noise, flicker noise, avalanche noise and capacitive crosstalk. Thermal noise is present in all passive resistive components which includes stray series resistances of inductors and capacitors. Thermal noise is caused by random thermal motion of electrons and occurs even when a resistor is electrically unloaded. Shot noise arises when charges cross a potential barrier, e.g. diode or transistor. Shot noise is also a random event and is a sum of many random current pulses.

Flicker noise, which is also called 1/f noise or contact noise, is present in all active devices. It is caused by traps which capture and release charge carriers randomly as current flows through them causing random fluctuation in the current itself. Flicker noise requires dc current and can also be found in some passive devices.

Avalanche noise is a form of noise, which is found in p-n-junctions. A p–n junction is a boundary or interface between two types of semiconductor material inside a single crystal of a semiconductor. Avalanche breakdown occurs when electrons under the influence of a strong electric field inside the space-charge layer, acquire enough kinetic energy to create additional pairs. The resulting current consists of randomly distributed noise spikes. Avalanche noise requires also current flow. However, avalanche noise is much more intense than shot noise. Zener diodes are best example of this noise type

Circuit crosstalk is unintentional coupling of voltages from other circuits to the measurement system output. The term crosstalk comes from the early analog phone lines where voices from neighboring lines could be heard due to electromagnetic coupling. Capacitive crosstalk can be avoided by protecting sensitive nodes, avoiding floating nodes, making rise and fall times as large as possible, not running wires together for a long distance and shielding of wires [19].

The performance of capacitive sensor is limited by external noise, internal noise, mechanical stability and environmental factors. When these limits are understood, and handled correctly, capacitive sensor design can be very stable and achieve low noise performance. However, observed noise levels are highly related to sampling rate of input signal. Figures 32 and 33 compare noise when sample rate is either 5kHz or 100 Hz. The noise level in Figure 32 is the unfiltered input for touch trigger algorithm. This is the derivative of pulse counts between two program cycles. Noise level in Figure 33 is filtered input for linear interpolation algorithm to construct force from frequency. This input is from pulse counter module, which gives average the frequency of input signal once every 10 milliseconds.

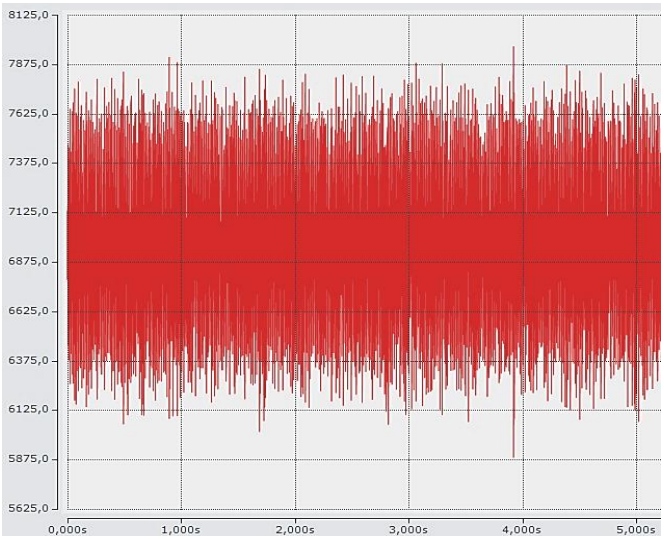

Figure 32. *Oscilloscope view of unfiltered raw pulse difference input with 5000 Hz sample rate*

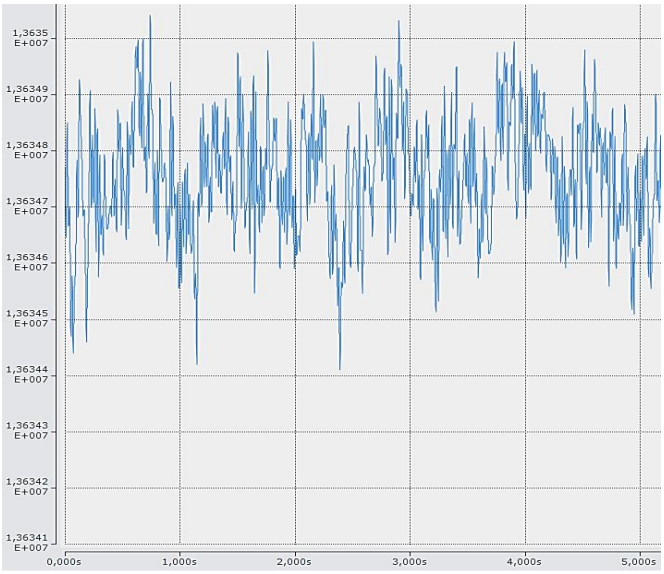

Figure 33. *Oscilloscope view of filtered input frequency with 100 Hz sample rate*

7.3 Sensitivity and hysteresis

Sensitivity indicates how much the output signal of the measurement system changes as a function of movement between two capacitive plates. The vertical movement of plates is directly related to how deep the robot travels through the surface of a device under test (DUT). Sensitivity is measured as frequency per millimeter when the system output is plotted against the gap size between the plates.

Hysteresis is the maximum difference between the frequency readings when the finger is at the same depth and under the same conditions and approaching from opposite directions. Figure 34 shows the frequency response and hysteresis of the sensor while going through the full range of motion in 0.1 mm steps. Sensor output sensitivity and hysteresis can be divided into two regions. The first one is the linear part, which begins when the sensor is at rest and ends when the finger has traveled 0.8 mm through the surface. This part behaves well and produces quite linear output to the applied force and has low hysteresis. The second region is nonlinear, starting at 0.8 mm and going all the way to the measurement range at 1.1 mm. Over the last 0.3 mm of travel the frequency decreases heavily, due to nature of capacitance. In this region, the capacitive sensor is the most sensitive and means also that the hysteresis is high. Hysteresis at the first region is 0.5% and from the second region 6.6%.

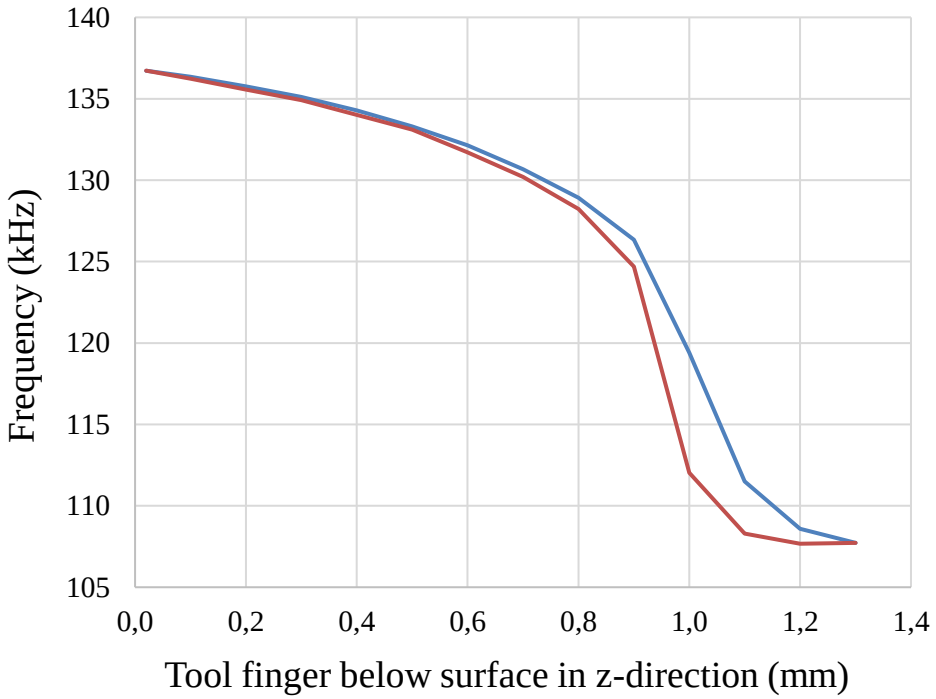

Figure 34. *Frequency sensitivity and hysteresis, blue represents the approach and orange represents the release*

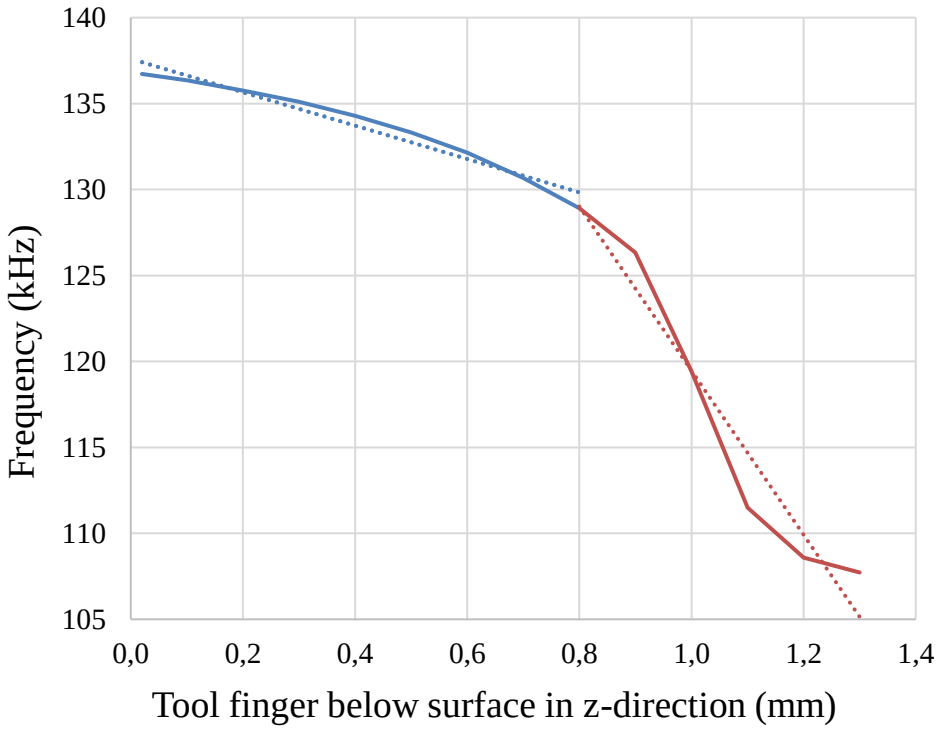

Figure 35. *Linearity error in two regions*

Sensitivity and linearity can be set during the mechanical setup of the sensor. If there is need for a highly linear output, then sensor can be adjusted to move within the first region. If greater sensitivity is needed, then the second setup is preferred.

The maximum deviation of the true response to the best fit straight line is called linearity error. This straight line is plotted in figure 35 in two parts to illustrate the difference between the linear and nonlinear properties of the system. The linearity error is $\pm$ 1% in the first region and $\pm$ 3% in the second region. For the full range of motion, the best fit straight line equation is $y = -23{,}589x + 142{,}28$, with linearity error of $\pm$ 5%.

7.4 Resolution

Resolution can be defined as the smallest reliable measurement a system can generate. The determining factors for the resolution are noise and the stability of the system. The electrical noise can be detected in output of the sensor as described before. Even if the gap between the two capacitive plates remains precisely the same, the output of the circuitry has a small amount of noise, which seems to indicate that that the gap is varying. This noise is inherent in the electronics and can be minimized, but never eliminated. The amount of noise in output is directly related to bandwidth. This means that noise is distributed over a wide range of frequencies. If higher frequencies can be filtered before the output, the result will be less noisy and better resolution.

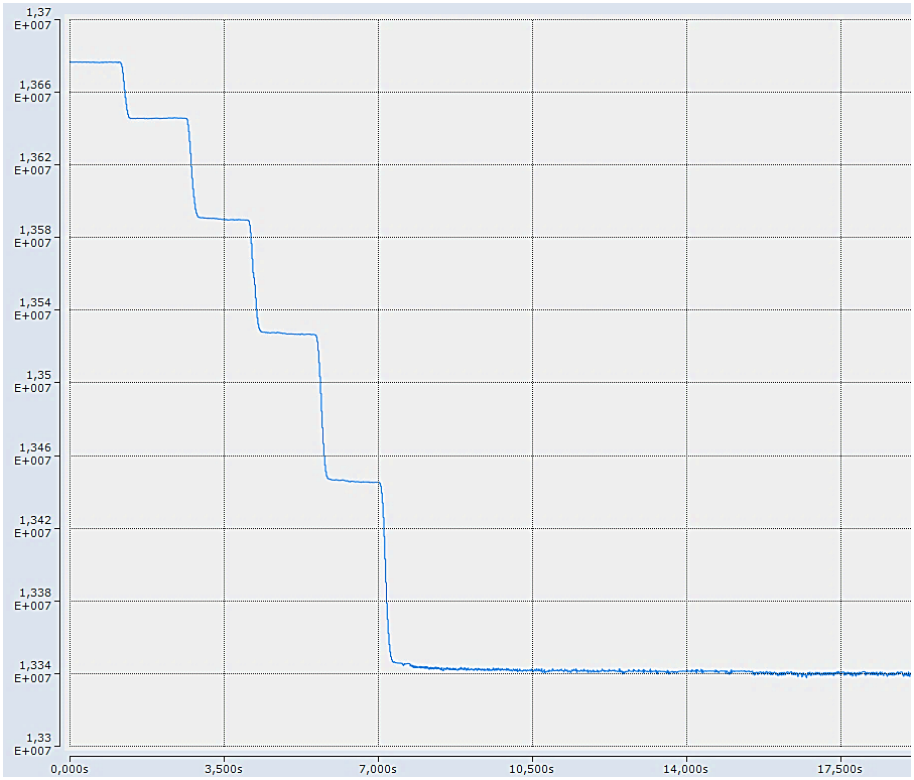

Figure 36. *Frequency response from 0 to 70 g in 0.5 mm transition of 0.1 mm steps*

Three actions have been taken into account to deal with noise and to maximize resolution. Firstly, a steel cover is placed over the capacitive pair to protect from parasitic capacitive coupling. Secondly, the signal is converted from analog to digital as close as possible to the location of measurement. Thirdly, the signal is low-pass filtered with the GMA.

This results in the frequency response displayed in Figure 36. This figure is an oscilloscope view and the horizontal axis is free running time axis. Frequency changes as a function of force, total force of 70 g is applied and it results in a total 5.6 kHz of change in frequency. The robot finger travels 0.5mm through the surface in 0.1mm steps. These steps can be clearly seen and contain very little noise or drift. The system is equipped with 0.1 mm thick spring steel sheets and is able to produce very linear force and capacitance response up to 0.8 N.

The resolution of the system is calculated as

$$Resolution = \frac{Noise\ RMS}{Sensitivity} = \frac{\frac{1}{2\sqrt{2}} * 0.3\ kHz}{8.2\ kHz/N} \approx 0.0258\ N \approx 2.6\ g \quad (8)$$

Here noise RMS is the peak-to-peak value from Figure 33. This noise is captured from a static hold at 0.26N with 0.1mm spring sheets. The sensitivity is the total change of frequency when force from 0 to 1N is applied.

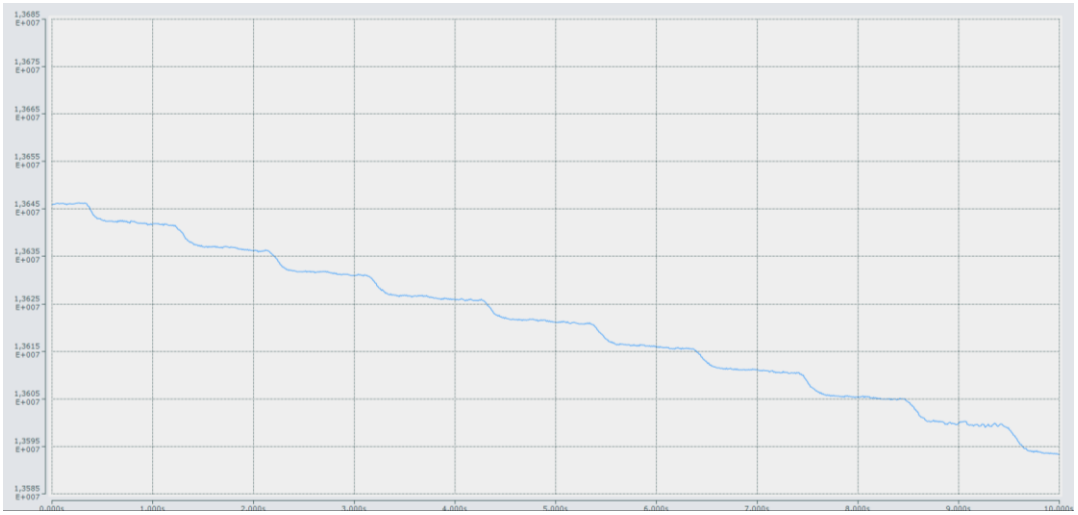

Figure 37. *Frequency response from 0 to 23.6 g 0.1 mm transition of 0.01 mm steps*

The estimated resolution of 2.6 g is tested in practice with a robot. In this test, a frequency response is plotted as a function of the applied force. Figure 37 is an oscilloscope view, where the horizontal axis is free running time axis. Force from 0 to 23.6 g is applied in total 10 steps of 0.01mm per transition. This is the smallest step in which the robot can move. Each step can be clearly seen, although slight drift can be noted. A rough resolution can be estimated from the oscilloscope view. If the total force is divided with the number of steps travelled, the resolution is $23.6\ \mathrm{g} / 10 \approx 2.36\ g$. It is even better than previously calculated and is limited by the robot resolution.

7.5 Precision and force characteristics

Precision is the maximum difference between output readings when the same amount of force is applied repeatedly under the same conditions. Here precision is measured by first loading the sensor under 50 grams of force with robot, then robot position is saved and driven back to the upper z-axis position where no force is detected. The saved robot position should give force of 50 grams every time its commanded to this z-axis position.

A total of 18 measurements were taken with 10 seconds of delay between each measurement, see Figure 38. This resulted in precision error of 1 gram illustrated in blue. However, there was a decreasing trend. Figure 38 presents the error and in reference Kern PCB scale in red. The scale error and the force correlate strongly. The scale error was measured during the 10 second delay between robot test cycle. During the total of 18 measurements the scale drifted from 0 g to 1.1 gram, resulting that Kern PCB scale is not good for a reference when determining the precision of the measurement. The precision results in Figure 38 are not reliable enough and the measurements should be repeated with better equipment.

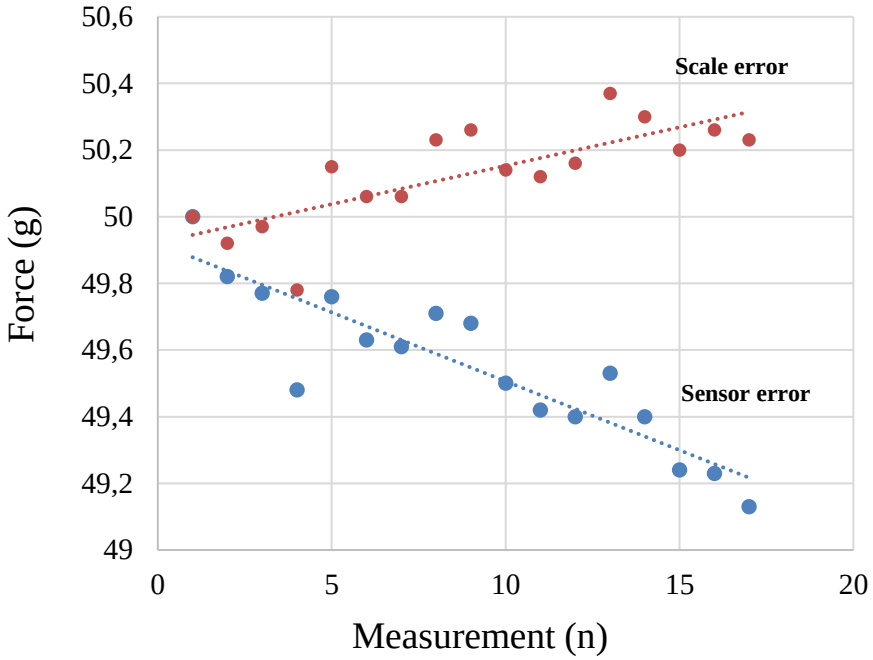

Figure 38. *Precision error*

The force characteristics of the sensor is directly related to shape, thickness and material properties of 1.4310 graded spring steel flexure pair. The force produced by the spring as a function of travel in millimeters is presented in Figure 39. In this figure, the linearity of the spring steel is clearly visible.

Another important feature is that the flexure in this form should produce a smooth, linear response up to 1 mm bend. Above 1 mm and up to the range at 1.35 mm, the spring steel behaves more aggressively and produces force with much higher slope. Therefore, the safe overload of the sensor is evaluated: According to these tests the maximum bend of the flexure must be limited to 1.35mm. The movement range can be kept under 1mm to achieve highly linear output and to keep the possible deformation risk minimal. Much like with frequency response, the force response can be divided into two regions where the hysteresis at the first region is 0.09 N and at the second region 0.46 N.

Figure 40 presents the force response of three assemblies in which the thickness of the spring steel flexure pair varies from 0.10 mm to 0.20 mm. This figure states that the material properties of spring steel are acceptable and the force output can be adjusted by the needs of the application.

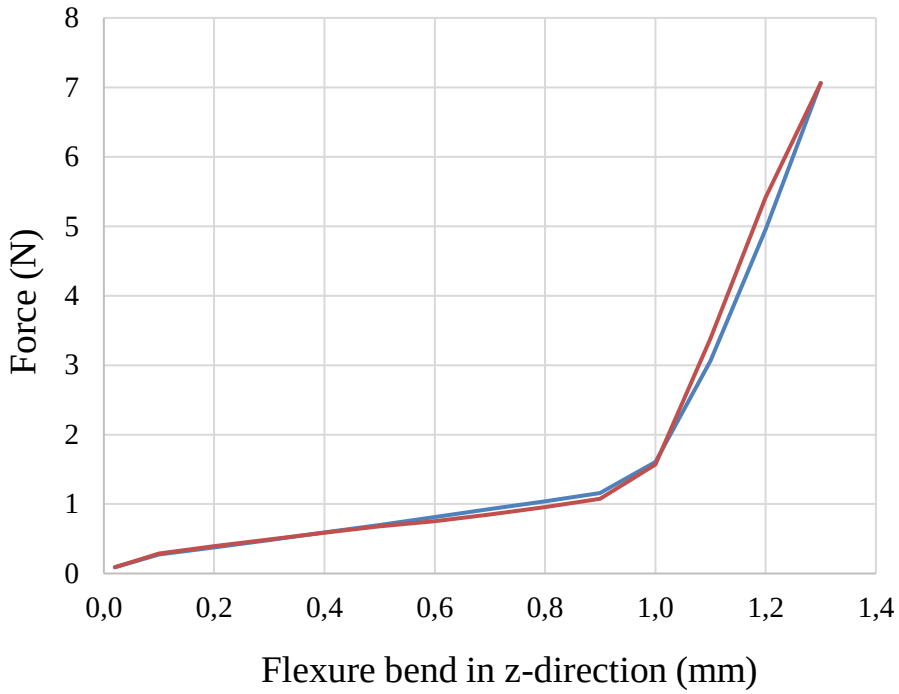

Figure 39. *Force sensitivity and hysteresis, blue represents the approach and orange represents the release*

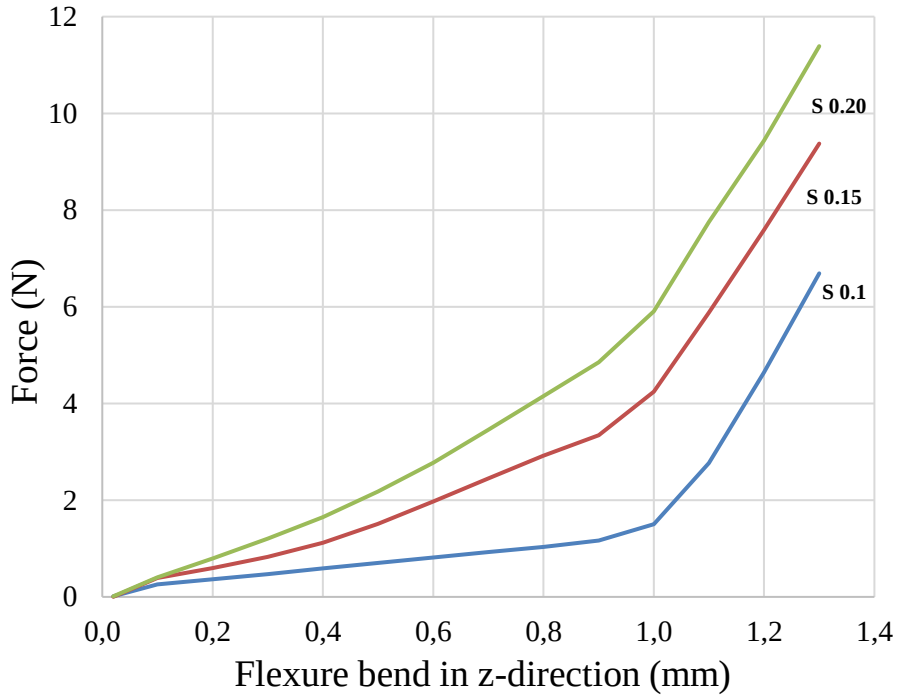

Figure 40. *Force sensitivity with different thicknesses of spring sheets*

7.6 Measurement for robot z-axis position

The original motivation for this thesis was to study touch sensing of z-axis position by a change in capacitance. The idea was to design and implement a sensor, tool mechanics and software sufficiently fast and sensitive for surface detection by touch. The theory and designs reported in the previous chapters result in following measurements presented in Figures 41, 42 and 43. In these figures the reaction time of the touch trigger algorithm is presented as histograms.

A total of 100 measurements were taken at different speeds of the robot. The test cycle was executed as follows: the robot approaches the calibration pad and places the tool above it. Then the robot begins the tap sequence and moves its z-axis up and down repeatedly, until the predetermined amount of 100 cycles is completed. Reaction time results are recorded as an array, which is then analyzed.

The time resolution of the measurements is 1.4 milliseconds as it is the cycle time of the touch trigger algorithm. Reaction time of the system should decrease when robot movement speed increases. From the results in Figure 41, it can be seen that although the median of the reaction time is below 2.43 ms, the speed of 100 mm/s causes a high deviation in the results. Recordings in this figure is with the highest speed what the robot can move. This causes unstable behavior in operation of the touch trigger algorithm and results in reaction times up to 4.8 ms. Thus, the maximum movement speed of 100mm/s in reaction time measurement is not recommended. If the operation of touch trigger algorithm could be trimmed to work better and more reliably with maximum speed, then faster reaction time would be achieved.

When the robot speed is decreased to 10 mm/s, operation of the touch trigger algorithm begins to stabilize and with lower speed, the system is capable of reacting touch events in under 3 milliseconds. Final results in Figure 43 were taken with the robot speed of 1 mm/s and these results are very similar to the results in Figure 42. Hence, also with this low speed, the reaction time is below 3 milliseconds.

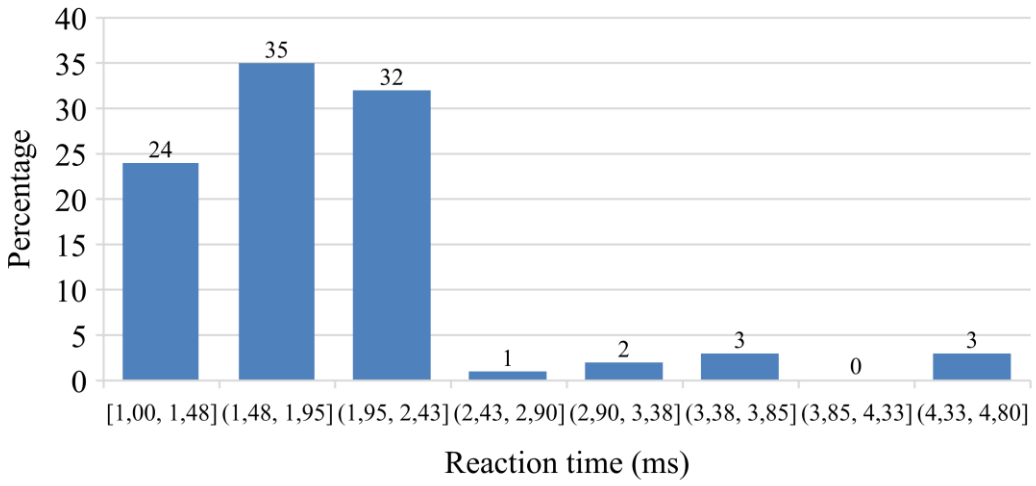

Figure 41. *Reaction time of the system at the speed of 100mm/s*

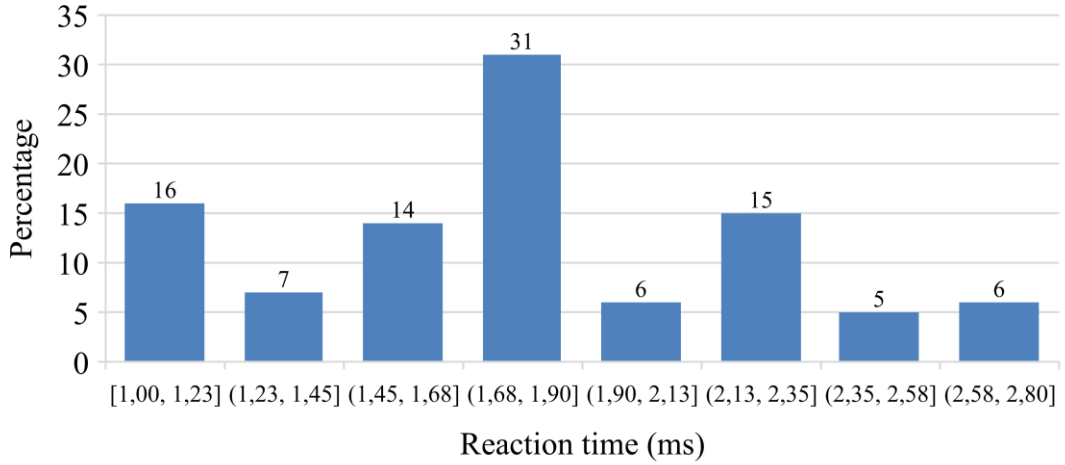

Figure 42. *Reaction time of the system at the speed of 1mm/s*

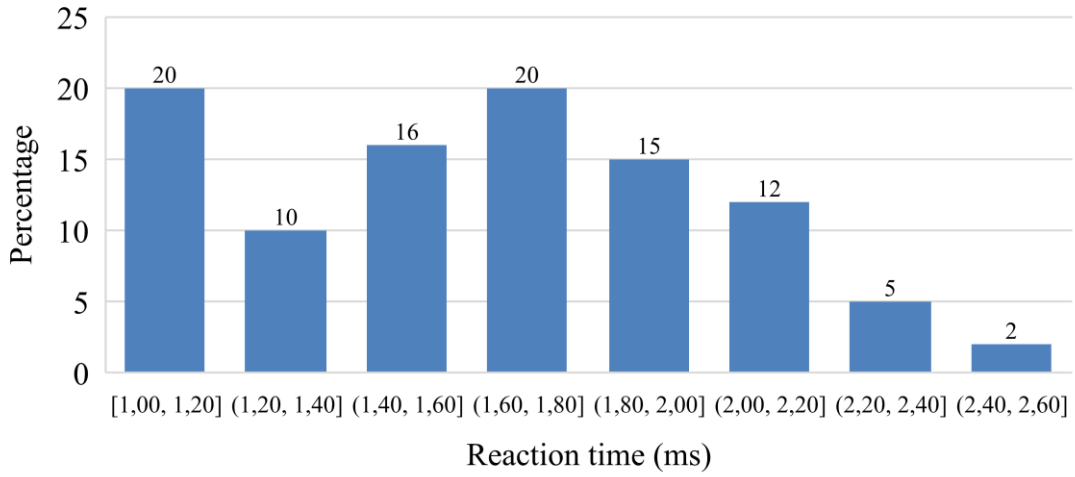

Figure 43. *Reaction time of the system at the speed of 1mm/s*

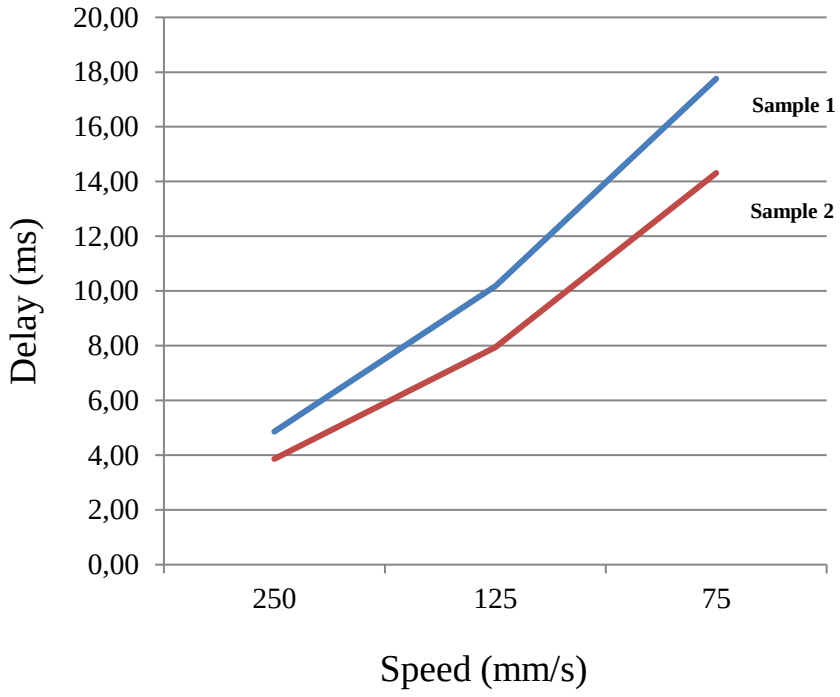

Figure 44. *Trigger delay median with optical triggers*

Figure 44 presents the results from One Finger and optical trigger driven against the calibration pad with different speeds. The results are from Optofidelity archives and the delay on vertical axis is the same as the reaction time in figures 41, 42 and 43. In Figure 44 even the fastest reaction time of slightly under 4 milliseconds is higher than what was achieved with the new capacitive measurement.

The old method for measuring the time instant of touch was by using the optical trigger in the robot tool, subtracting the delay, Figure 44, and trusting the robot speed to be constant. By this old method, the touch detection is rather far from real time needs but the results are used when postprocessing the data.

8. CONCLUSIONS

The goal of this Master of Science thesis was to design and implement a robot end effector with a capacitive tactile sensor to measure the robot z-axis position. This goal was successfully accomplished. The resulting physical prototype shown as reported in this document is the property of Optofidelity and is the proof of the completing the task.

The final version of the tool and sensor mechanics is the result of several iterative computer aided design cycles. The designed prototype is a proof of concept that capacitance can be used in a tactile force sensing. The results of the measurements for evaluating the sensor can be summarized in a following way. The sensor equipped with 0.1 mm spring steel flexure pair is capable to measure forces from 0 g to 70 g with a resolution of 2.36g, precision of 1 g, hysteresis of 0.5% and linearity error of ± 1%. Results were achieved utilizing the linear region of the sensor. The resolution of the measurements was limited by the robot's movement resolution. The sensor mechanics do not limit the maximum force. Forces up to 1100 g were reported with spring steel flexure thickness of 0.2 mm. The original motivation was to study touch detection of z-axis position. In such measurements, a reaction time under 3 ms was achieved. This means that the new design outperformed the previous system.

At the time of writing this thesis, a design to implement a capacitive force measurement with spring steel flexure mechanics for a commercial robot has been proposed. It would be the first of a kind to be applied in a customer project. The research carried out in this thesis contains valuable information and experience of the capabilities of the system how it should work.

As always, the designed mechanics are application driven but the principles of flexure mechanics are generic. On the electronics side a differential capacitive measurement of two capacitive pairs could also be used. The system for pulse counting may change from Beckhoff to something else, but the working principle will not change.

REFERENCES

[1] S. R. Dahiya, M. Valle, Robotic Tactile Sensing, Technologies and System, Springer Dordrecht Heidelberg New York, London, 2013, pp 81-101

[2] A. R. Russell, J. A. Wijaya, Object Location and Recognition using Whisker Sensors (Accessed: 12-3-2017), Available: https://pdfs.semanticscholar.org/618b/7a3912df03e99a52ab5e623282a53ecfab15.pdf

[3] Honeywell limit switch & whisker end effector (Accessed: 12-3-2017), Available: https://sensing.honeywell.com/index.php?ci_id=144406

[4] Uneo FSR sensor (Accessed: 12-3-2017), Available: http://www.uneotech.com/uneo/us/product-en.html

[5] Gauge Factor and Stretch ability of Silicon-on-Polymer Strain Gauges (Accessed 16-3-2017), Available: https://www.ncbi.nlm.nih.gov/pmc/articles/PMC3758612/

[6] National Instruments, Measuring Strain with Strain Gages (Accessed 12-3-2017), Available: http://www.ni.com/white-paper/3642/en/

[7] Futek S-beam LSB200 load cell (Accessed: 12-3-2017), Available: http://www.futek.com/files/pdf/Product%20Drawings/lsb200.pdf

[8] Tekscan piezoresistive FlexiForce A101 sensor (Accessed: 12-3-2017), Available: https://www.tekscan.com/products-solutions/force-sensors/a101?tab=specifications

[9] Noliac piezoelectric accelometer (Accessed: 16-3-2017), Available: http://www.noliac.com/products/sensors/kind/productpage/pageaction/pdf/pagecontroller/Page/show/tutorial-piezo-basics/pagetype/67589/

[10] A. Tandon, P. Shukla, H. K. Patel, Review of Transduction Techniques for Tactile Sensors and a Comparative Analysis of Commercial Sensors, 2nd International Conference on Multidisciplinary Research & Practice, 2015

[11] M. Ohka, H. Kobayashi, J. Takata, Y. Mitsuya, Sensing Precision of an Optical Three-axis Tactile Sensor for a Robotic Finger, The 15th IEEE International Symposium on Robot and Human Interactive Communication (RO-MAN06), Hatfield, UK, September 6-8, 2006, Available: http://ieeexplore.ieee.org/document/4107811/

[12] J.-S. Heo, J.-H. Chung, J.-J. Lee, Tactile sensor arrays using fiber Bragg grating sensors, Sens. Actuators A, Phys. 126, (2006), Available: http://www.sciencedirect.com/science/article/pii/S0924424705006084

[13] SensorWiki Hall effect (Accessed 12-3-2017), Available: http://sensor-wiki.org/doku.php/sensors/hall_effect

[14] Loadstar sensors, What is a Load Cell (Accessed: 12-3-2017), Available: http://www.loadstarsensors.com/what-is-a-load-cell.html

[15] SingleTact capacitive force sensor (Accessed: 12-3-2017), Available: https://www.singletact.com/SingleTact_Datasheet.pdf

[16] Relative Permittivity of Materials (Accessed 5-4-2017), Available: https://en.wikipedia.org/wiki/Relative_permittivity

[17] Strain Gauges (Accessed 25-3-2016), Available: https://www.allaboutcircuits.com/textbook/direct-current/chpt-9/strain-gauges/

[18] Data Sheet Spring Steel Wire 1.4310 (Accessed 26-3-2017), Available: http://www.stahlbecker.de/sites/stahlbecker.de/files/datasheets/datasheet_sping_steel_wire_1.4310.pdf

[19] S. Franco, Design with Operational Amplifiers and Analog Integrated Circuits, McGraw-Hill, New York, 2002, pp 311-346 & 465-471

[20] 555-timer Circuits (Accessed 28-3-2017), Available: http://www.555-timer-circuits.com/

[21] 555 Timer Tutorial (Accessed 29-3-2017), Available: http://www.electronics-tutorials.ws/waveforms/555_timer.html

[22] Advantech ARK-1123 Embedded PC (Accessed 15-3-2017), Available: http://www.advantech.com/products/92d96fda-cdd3-409d-aae5-2e516c0f1b01/ark-1123c/mod_0b91165c-aa8c-485d-8d25-fde6f88f4873

[23] Beckhoff EK1100 EtherCAT coupler (Accessed 15-3-2017), Available: https://www.beckhoff.com/english.asp?ethercat/ek1100.htm

[24] Beckhoff EL5101 Incremental encoder (Accessed 15-3-2017), Available: https://www.beckhoff.com/el5101/

[25] Beckhoff EL1094 Negative switching digital input terminal (Accessed 15-3-2017), Available: https://www.beckhoff.com/english.asp?ethercat/el1094.htm

[26] Beckhoff EL2008 Digital output terminal (Accessed 15-3-2017), Available: http://www.beckhoff.fi/english.asp?ethercat/el2008.htm

[27] Geometric Moving Average (Accessed 15-3-2017), Available: https://en.wikipedia.org/wiki/Moving_average

[28] Linear Interpolation (Accessed 5-4-2016), Available: https://en.wikipedia.org/wiki/Linear_interpolation

[29] O. Aumala, H. Ihalainen, H. Jokinen & J. Kortelainen, Mittaussignaalien käsittely, Pressus Oy Tampere 1998, pp 23-68

APPENDIX A: ILLUSTRATION OF DESIGNED TOOL